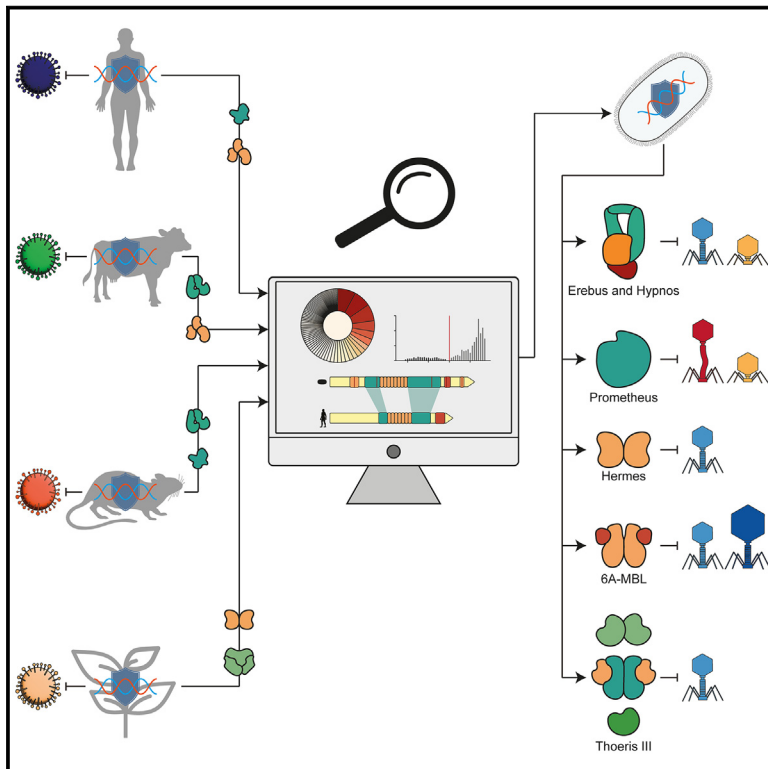


Cell Host & Microbe

Bacterial homologs of innate eukaryotic antiviral defenses with anti-phage activity highlight shared evolutionary roots of viral defenses

Graphical abstract



Authors

Daan F. van den Berg, Ana Rita Costa, Jelger Q. Esser, ..., Adja Damba Zoumaro-Djayoon, Pieter-Jan Haas, Stan J.J. Brouns

Correspondence

stanbrouns@gmail.com

In brief

Van den Berg et al. discover several bacterial homologs of eukaryotic antiviral defenses and demonstrate the anti-phage activity for six previously uncharacterized systems. These findings highlight the shared evolutionary roots and common mechanisms for viral defense across prokaryotes and eukaryotes.

Highlights

- Bacterial homologs of eukaryotic innate immunity genes examined in *P. aeruginosa*
- Over 400 eukaryotic-like bacterial antiviral candidates were identified
- Six eukaryotic-like phage defense systems validated to have strong anti-phage activity
- Findings underscore the shared evolutionary roots of viral defenses across the domains

Article

Bacterial homologs of innate eukaryotic antiviral defenses with anti-phage activity highlight shared evolutionary roots of viral defenses

Daan F. van den Berg,^{1,2,4} Ana Rita Costa,^{1,2,4} Jelger Q. Esser,^{1,2,4} Ilinka Stanciu,^{1,2} Jasper Q. Geissler,^{1,2} Adja Damba Zoumaro-Djyoon,¹ Pieter-Jan Haas,³ and Stan J.J. Brouns^{1,2,5,*}

¹Department of Bionanoscience, Delft University of Technology, 2629 HZ Delft, the Netherlands

²Kavli Institute of Nanoscience, Delft, the Netherlands

³Medical Microbiology, University Medical Center Utrecht, Utrecht University, 3584 CX Utrecht, the Netherlands

⁴These authors contributed equally

⁵Lead contact

*Correspondence: stanbrouns@gmail.com
<https://doi.org/10.1016/j.chom.2024.07.007>

SUMMARY

Prokaryotes have evolved a multitude of defense systems to protect against phage predation. Some of these resemble eukaryotic genes involved in antiviral responses. Here, we set out to systematically project the current knowledge of eukaryotic-like antiviral defense systems onto prokaryotic genomes, using *Pseudomonas aeruginosa* as a model organism. Searching for phage defense systems related to innate antiviral genes from vertebrates and plants, we uncovered over 450 candidates. We validated six of these phage defense systems, including factors preventing viral attachment, R-loop-acting enzymes, the inflammasome, ubiquitin pathway, and pathogen recognition signaling. Collectively, these defense systems support the concept of deep evolutionary links and shared antiviral mechanisms between prokaryotes and eukaryotes.

INTRODUCTION

Prokaryotes are subject to persistent predation by bacteriophages, driving the evolution of diverse host defense systems and phage-encoded countermeasures to evade these defense systems.¹ This ongoing arms race relies on the rapid turnover of defensive and counter-defensive mechanisms,^{2,3} and is facilitated by mobile genetic elements (MGEs) that encode the large majority of the known anti-phage defense mechanisms.⁴ These MGEs integrate into genetic hotspots within the genome, known as defense islands.^{3–10} Searching for defense systems within these defense islands has significantly expanded our understanding of the prokaryotic immune repertoire, leading to the discovery of more than 100 defense mechanisms in the past 6 years.^{5–7,11,12}

A few of these defense mechanisms exhibit a striking resemblance to eukaryotic genes involved in antiviral response, such as Toll/interleukin-1 receptor (TIR), Argonaute, Gasdermin, cyclic guanosine monophosphate-adenosine monophosphate synthase (cGAS), and Dynamin-like (Mx) proteins.^{5,7,13–19} These findings highlight shared evolutionary strategies in the context of the perpetual struggle against viral pathogens, bridging the gap between prokaryotic and eukaryotic immune systems. Further investigating the link between prokaryotic and eukaryotic immune systems can provide valuable insights into the evolutionary origins and underlying mechanisms of eukaryotic immune responses.

Motivated by these factors, we set out to systematically project the current knowledge of eukaryotic-like antiviral defense systems onto prokaryotic genomes using *Pseudomonas aeruginosa* as a model organism, a bacterium known for its exceptional diversity and abundance of defense systems.^{8,10,20} Here, we report that inositol-monophosphate phosphatase (IMPase) Hermes, a plant-tolerance-like factor, provides anti-phage defense via modifications of the cell surface that prevent viral adsorption. We also report a DNA replication helicase/nuclease 2 (DNA2)-containing anti-phage defense protein (Prometheus) that is similar to eukaryotic antiviral R-loop acting enzymes, important components of the innate immune system of various eukaryotes.^{21–32} In addition, we discovered four eukaryotic-like anti-phage defense systems, two of which are similar to antiviral inflammasome components featuring a new clade of NACHT domain-containing proteins with a distinct architecture and two previously unknown anti-phage effectors: NucS and SfsA (bNACHT Erebus and bNACHT Hypnos). Moreover, we discovered another defense system that contains eukaryotic-like ubiquitin-related components, consisting of a fused E1-E2-JAB protein combined with a metallo-beta-lactamase fold (MBL-fold) protein (6A-MBL). This defense system is a distant homolog of the pathogen receptor signaling of Toll-like receptors and introduces a new subtype of the TIR-containing Thoeris anti-phage defense family. Thoeris type III is characterized by the presence of a ThsB-like protein with a NucS

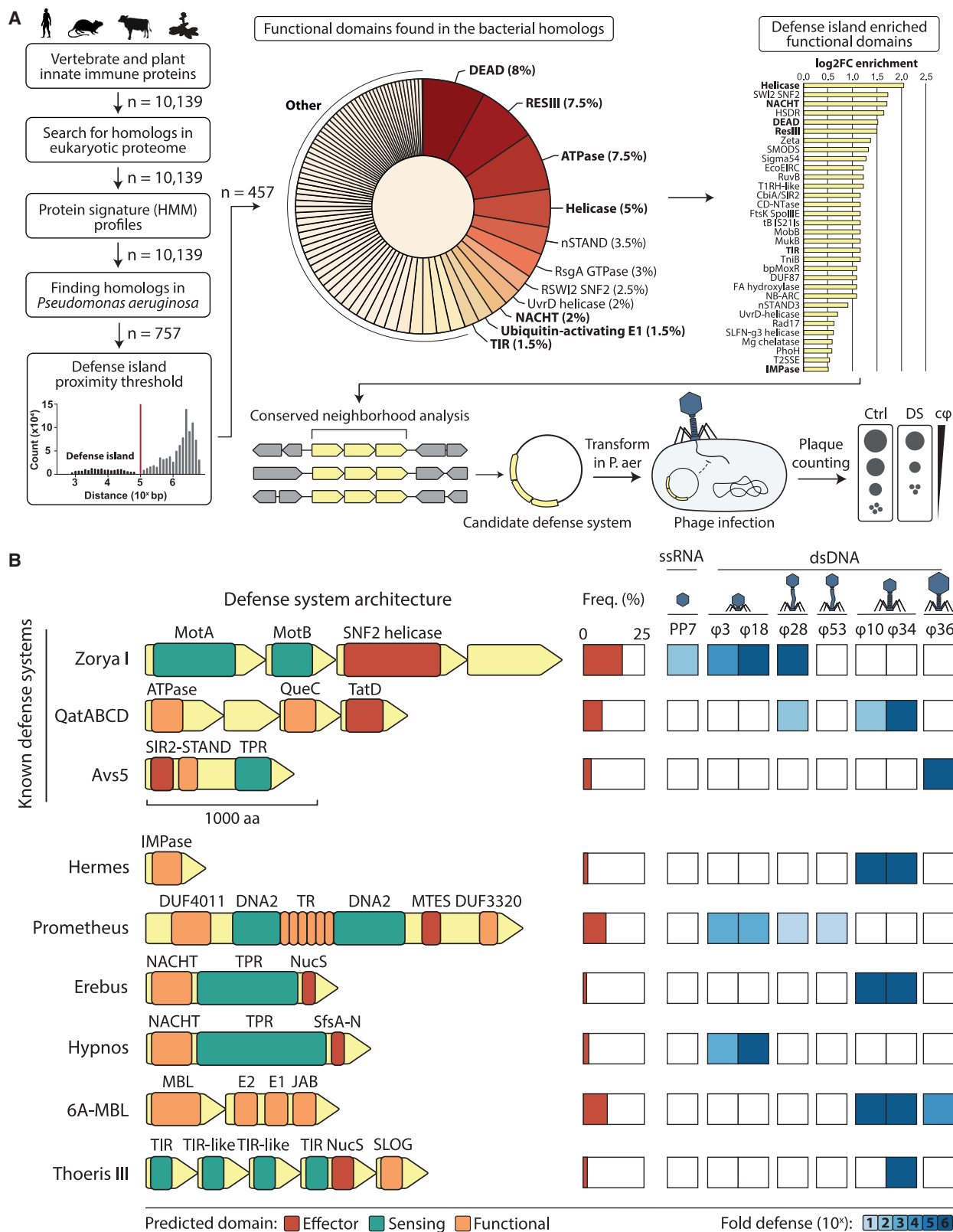


Figure 1. Anti-phage activity of defense systems identified in *P. aeruginosa* that are homologous to eukaryotic antiviral immunity
(A) Strategy used for the identification of bacterial homologs of proteins involved in eukaryotic innate immunity, from vertebrates (*Homo sapiens*, *Mus musculus*, and *Bos taurus*; InnateDB) and plants (363 species; PRGdb) that are in proximity of known defense systems. Shown are the functional domains found within these

(legend continued on next page)

endonuclease effector domain and an uncharacterized SMF/DprA-LOG (SLOG) domain protein from a lineage not previously linked to Thoeris systems.

These defense systems can be found in up to 11 bacterial phyla, being the most prevalent among Proteobacteria, and enhance our understanding of the complex connection between bacterial and eukaryotic immune systems.

RESULTS

Eukaryotic-like antiviral homologs show anti-phage activity

To identify eukaryotic-like defense systems in *P. aeruginosa*, we used the entire set of experimentally verified protein sequences associated with eukaryotic innate immunity from the InnateDB³³ as our starting database ($n = 10,139$), including *Homo sapiens* ($n = 7,886$), *Mus musculus* ($n = 2,100$), and *Bos taurus* ($n = 153$) (Table S1). Additionally, we applied DRAGO3³⁴ to search for plant pathogen recognition proteins and a custom literature-based list of functional domains associated with plant and vertebrate innate immunity (Table S1). We used this starting set of proteins as a seed to identify all eukaryotic homologs included in Eukprot³⁵ with the use of MMseqs2 (easy-cluster)³⁶ and subsequently built a hidden Markov model (HMM) protein signature from an average of 218 sequences for each validated innate immune protein. By applying these signatures to all representative proteins within regions of genomic plasticity of *P. aeruginosa*, we identified 757 homologs, indicating that 11.2% of the representative genes within the overall pangenome of *P. aeruginosa* exhibit similarity to eukaryotic proteins associated with innate immunity (Figure 1A; Table S2).

To narrow down the selection of these eukaryotic homologs for testing possible antiphage activity, we focused on gene clusters that occur in the proximity of known defense systems. The resulting 457 homologs contained a large range of functional domains, including the most abundant type III restriction enzyme (RESIII) and DEAD/DEAH box helicase (DEAD). These two functional domains are also present within the most notable nucleotide-acting antiviral defenses within eukaryotes, including retinoic acid-inducible gene I (RIG-I) and endoribonuclease Dicer.^{37,38} To assess the likelihood of these functional domains being associated with anti-phage activity, we determined if they were enriched in defense islands compared with other genomic regions. This was achieved by computing the log-fold change (\log_2FC) in the prevalence of the domain within proximity to known defense systems (<0.1 Mb) compared with its prevalence at greater distances (>0.1 Mb) (Figure 1A). The 0.1 Mb threshold was determined based on the distances observed between known defense systems within defense islands of *P. aeruginosa*, which align with those previously reported in

E. coli.⁴ Among the eukaryotic antiviral associated functional domains that are most enriched in phage defense islands, several were already known to be shared by bacterial and eukaryotic antiviral strategies. These included components involved in pathogen recognition, such as signal transduction ATPases with numerous domain (STAND) proteins and cGAS/DncV-like nucleotidyltransferases (CD-NTases) involved in the eukaryotic antiviral pathway of cGAS.^{39–41}

We then set out to experimentally test the anti-phage activity of eleven conserved gene clusters that contain at least one of the most enriched functional domains, including DEAD, RESIII, ATPase, Helicase, NACHT, Ubiquitin-activating E1, TIR, and the less common IMPase, by introducing the gene clusters with their native promoters into *P. aeruginosa* strain PAO1 on a low-copy plasmid¹⁰ (Figure 1B; Table 1). These strains were subsequently challenged with a set of representative *P. aeruginosa* phages from six taxonomic groups (Figure 1A),^{10,42} revealing six eukaryotic-like defense systems. Remarkably, all except one (Prometheus) demonstrated a complete inhibition (more than 10^6 -fold) of phage propagation for at least one phage, including Hermes, bNACHT Erebus, bNACHT Hypnos, 6A-MBL, and Thoeris III (Figure 1B). Together, these findings confirm the discovery of six defense systems with eukaryotic-like antiviral functional domains. We will discuss these in more detail in the subsequent sections.

Hermes is a homolog of eukaryotic immune IMPases that prevents phage adsorption

Hermes was named after the Greek deity that functions as the messenger of the gods and consists of one gene with an inositol monophosphatase (IMPase) functional domain (Figure 2A; Table 1). Hermes provides complete protection against myophages $\phi Pa10$ and $\phi Pa34$ from the *Pbunavirus* genus, causing a reduction in phage infectivity of at least 10^6 -fold in efficiency of plating assays (Figure 1B), reducing phage propagation in liquid cultures by 10^2 -fold (Figures 2B and S1A), and allowing an almost complete recovery of bacterial growth under phage predation (Figure 2C). A point mutation in a conserved aspartic acid residue (D89A) in the predicted IMPase active site completely abolished phage protection (Figure 2D). Hermes shows strong similarity to eukaryotic IMPases (inositol monophosphatase 1, IMPA) involved in innate antiviral responses, both structurally (distance matrix alignment [DALI] Z score: 32.8) and at the sequence level (20%–30% pident) (Figures S1B and S1C). Hermes also shares resemblance with the bacterial IMPase SuhB, a constituent of the core genome of *P. aeruginosa*^{43,44} (31% pident; DALI Z score: 30.0) (Figure S1B). Similar to SuhB and IMPA, Hermes is predicted to form a dimer structure (Figure S1D). Noteworthy, phylogenetic analyses suggest that Hermes is the closest bacterial relative to the eukaryotic IMPase

homologs, in addition to their prevalence in the *P. aeruginosa* homolog set in comparison to homologs more distant from defense systems (\log_2FC). A subset of conserved gene clusters containing these enriched functional domains was selected for subsequent assessment of their potential antiviral activity (in bold). The candidate defense systems were cloned with their native promoters into pUCP20 and then introduced into the *P. aeruginosa* strain PAO1. The anti-phage activity of the candidate defense systems was assessed using efficiency of plating assays.

(B) The anti-phage activity of the defense systems against a panel of eight phages from six distinct taxonomic groups, measured by efficiency of plating assays. Previously validated defense systems¹⁰ were included as controls. The defense system architecture shows functional domains, color-coded based on their predicted function (Table 1). Genes are drawn to scale, with the scale bar representing 1,000 amino acids. The bar graph shows the abundance of the defense systems in *P. aeruginosa* genomes of RefSeq.

Table 1. Genes and functional domains of the eukaryotic-like defense systems

| Defense system | Gene | Functional domain(s) | Clusters of Orthologous Genes (COG)/Pfam/Conserved Domains Database (CDD) | Best eukaryotic hit |
|------------------|---------------|--|---|---------------------|
| Hermes | <i>hrsA</i> | IMPase ^a | PF00459, cl00289 | IMPA1/2 |
| Prometheus | <i>proA</i> | DUF4011, DNA2, ^{a,b} tandem repeat (TR), ^c REase_MTES, DUF3320 | PF13195, PF18741, COG1112, PF11784 | MOV-10 RNA helicase |
| bNACHT Erebus | <i>eruA</i> | NACHT, ^{a,b} TPR, ^{a,c} NucS endonuclease ^d | cl26020, PF05729, PF13176, PF01939 | NLRC4 inflammasome |
| bNACHT Hypnos | <i>hyoA</i> | NACHT, ^{a,b} TPR, ^{a,c} SfsA-N DNA-binding ^d | cl26020, PF05729, PF13176, PF17746 | NLRC4 inflammasome |
| 6A-MBL | <i>mbfB</i> | ComA-like MBL-fold | cd07731 | – |
| | <i>cap2-3</i> | E2, ^a E1, ^a JAB ^a | PF14457, cl37499, PF14464 | UBE2E1 |
| Thoeris type III | <i>thcB1</i> | Cap12-like TIR ^a | PF01582 | SARM1 |
| | <i>thcB2</i> | TIR-like DUF1863 | PF08937 | – |
| | <i>thcB3</i> | TIR-like DUF1863 | PF08937 | – |
| | <i>thcB4</i> | ThsB-like TIR, ^{a,b} NucS endonuclease ^d | PF01582 | SARM1 TLR adaptor |
| | <i>thcA</i> | SLOG | PF18178 | – |

^aFunctional domain associated with eukaryotic antiviral response.

^bFunctional domain is present in the eukaryotic homolog.

^cPredicted with HHrepID.

^dPredicted with Foldseek or DALI.

family (Figure 2E).^{45–50} Eukaryotic IMPases typically function by dephosphorylating IMPase to produce myo-inositol, which serves as the precursor for key signaling molecules in several cellular processes, including apoptosis, stress tolerance, cyclic AMP (cAMP) production, and cell growth.^{45–47} In addition, eukaryotic IMPases provide viral defense through affecting viral attachment and interfere with viral packaging by altering lipid composition and expression of viral receptors.⁵¹ In bacteria and archaea, inositol-containing molecules have been linked to osmotic balance,⁵² capsule (CPS) expression,⁵³ and the biosynthesis of membrane phosphatidylinositols, which can be modified to anchor proteins or complex carbohydrates to cell surfaces.⁵⁴ Given the role of the IMPase family in surface alterations in both eukaryotes and prokaryotes, we hypothesized that Hermes-mediated phage defense might involve surface modifications preventing phage adsorption. Further investigations revealed that *Pbunavirus* φPa34 completely failed to adsorb to Hermes cells, while *PhiKzvirus* φPa36 adsorbed similarly to control and Hermes cells (Figure 2F).

Analysis of cell surface components, including CPS (Figure 2G), lipopolysaccharides (LPSS, Figure 2H), and outer membrane proteins (Figure S1E), demonstrated alterations at all levels in cells expressing Hermes. Because *Pbunavirus* have been shown to use LPS as their receptor,^{55,56} we hypothesized that modifications in LPS could account for the observed inability of φPa34 to adsorb to Hermes cells. Strikingly, while φPa34 successfully adsorbed to LPS extracted from control and Hermes D89A cells (which also contained CPS), no adsorption was observed for LPS derived from Hermes-expressing cells (Figure 2I), supporting our hypothesis that Hermes provides phage defense through LPS and/or CPS alterations at the cell surface via IMPase-dependent pathways.

To gain insights into the substrate specificity of Hermes, we inspected the binding pocket and compared the conserved residues among Hermes, IMPA1, and SuhB (Figure S1B). We observed that Ala90 in the active site of Hermes differs from the corresponding Thr95 in IMPA1 and Thr109 in SuhB, which are critical residues for sequestering magnesium ions that catalyze the hydrolysis of IMPase into myo-inositol.⁴⁹ This variation suggests that Hermes may target a related but distinct substrate, a hypothesis further supported by mass spectrometry analysis, which showed identical levels of IMPase and myo-inositol in both Hermes-expressing and control cells (Figure S1F).

Collectively, our findings reveal a conserved mechanism of antiviral defense by IMPase-relatives in both prokaryotes and eukaryotes, which prevents viral adsorption through alterations of the cell surface (Figure 2J).

Prometheus is a bacterial homolog of human DNA2 antiviral defense genes

Prometheus, named after the Greek titan associated with the creation and protection of humanity, is part of the bacterial DNA2-like enzyme (Bad) family,⁵⁷ which also includes anti-phage genes *hhe*,⁶ *Mokosh MkoA*, and *Mokosh MkoC*.⁷ Prometheus is composed of one very large open reading frame encoding a protein of 2,221 amino acids with four predicted functional domains: DUF4011, DUF3320, DNA2 helicase/nuclease, and REase MTEs domains (Figure 3A; Table 1).

The DNA2 domain is shared with several human antiviral genes, including NFX1-type zinc-finger-containing protein 1 (ZNF1), Senataxin (SETX), DNA-binding protein SMUBP-2 (IGHMBP2), helicase with zinc finger 2 (HELZ2), Moloney leukemia virus 10 homolog (MOV-10), and UP Frameshift 1 helicase (Upf1) (Figures 3A, 3B, and S2A).^{21,25–32} These human genes

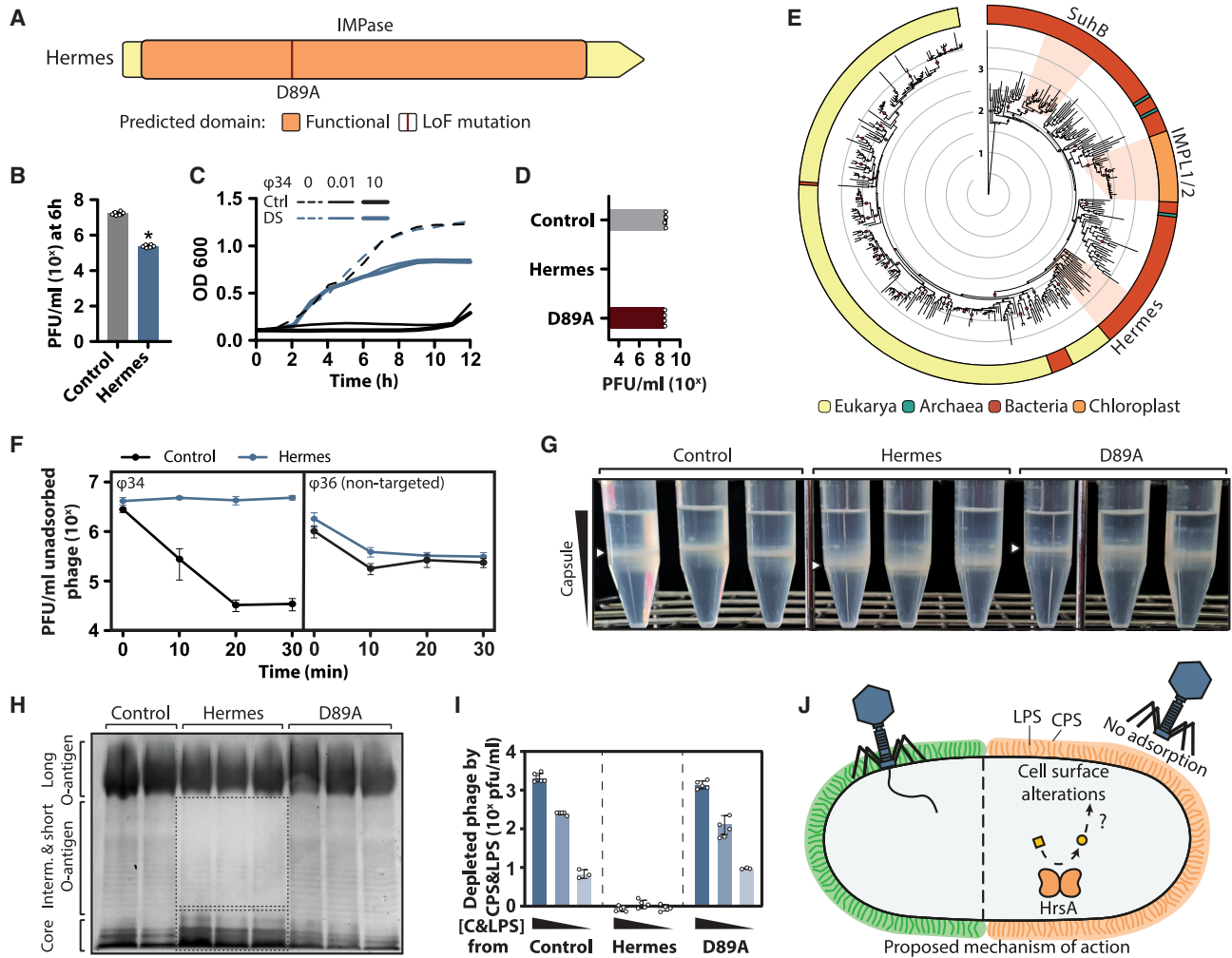


Figure 2. Hermes is an anti-phage defense system with strong similarities to eukaryotic antiviral IMPase proteins by preventing phage adsorption

(A) The functional domains of Hermes and mutation sites tested in (D). LoF, loss of function.

(B) Impact of Hermes on phage propagation in liquid culture. The propagation of phage ϕ Pa34 was monitored over time, and the 6 h time point is shown here, with all data points displayed in Figure S1A. The control bar represents phage propagation in PAO1 containing an empty plasmid. Bars represent the average of six biological replicates with individual points and standard deviation shown. * $p < 0.05$.

(C) Effect of the defense system on bacterial growth upon phage infection. PAO1 cells containing an empty plasmid (control) or Hermes (defense system [DS]) were infected with phage ϕ Pa34 at low (0.01) and high (10) multiplicity of infection, and their growth was monitored for a period of 12 h. Curves represent the average of three biological replicates.

(D) Effect of mutations in the functional domains of the defense system on phage protection. The infectivity of phage ϕ Pa34 on PAO1 cells containing an empty plasmid (control), Hermes, or Hermes with point mutations was assessed by plaque assay. Bars represent the average of three biological replicates with individual points and standard deviation shown.

(E) Phylogenetic tree of IMPase-containing proteins. The phylogenetic tree of 366 representative proteins was inferred and bootstrapped using IQ-Tree2 and rooted with a fructose-1,6-bisphosphatase class 1 protein (FBPase class 1; GenBank: CEI80039.1) from *P. aeruginosa*. The clades of human IMPA1 and IMPA2, plant IMPL1 and IMPL2, and prokaryotic HrsA and SuhB are indicated in the tree.

(F) Adsorption of phage ϕ Pa34 to cells harboring either an empty plasmid (control) or Hermes. The values represent the average concentration of unbound phage during a 30-min incubation period, for three biological replicates, with standard deviations shown. Adsorption of phage ϕ Pa36, which is not targeted by Hermes, serves as a control.

(G) Capsule amount produced by cells harboring empty plasmid (control), Hermes, or Hermes with a point mutation (D89A). The capsule amount was determined using Percoll density gradients (40%, 60%, and 80%). The location of the capsule band is highlighted with a white triangle.

(H) Lipopolysaccharide (LPS) fractions extracted from cells expressing empty plasmid (control), Hermes, or Hermes with a point mutation (D89A). LPS samples were separated on a 12% SDS-PAGE gel and stained with SYPRO Ruby. Regions exhibiting band intensity differences in Hermes cells compared with control and D89A cells are indicated by dashed rectangles.

(legend continued on next page)

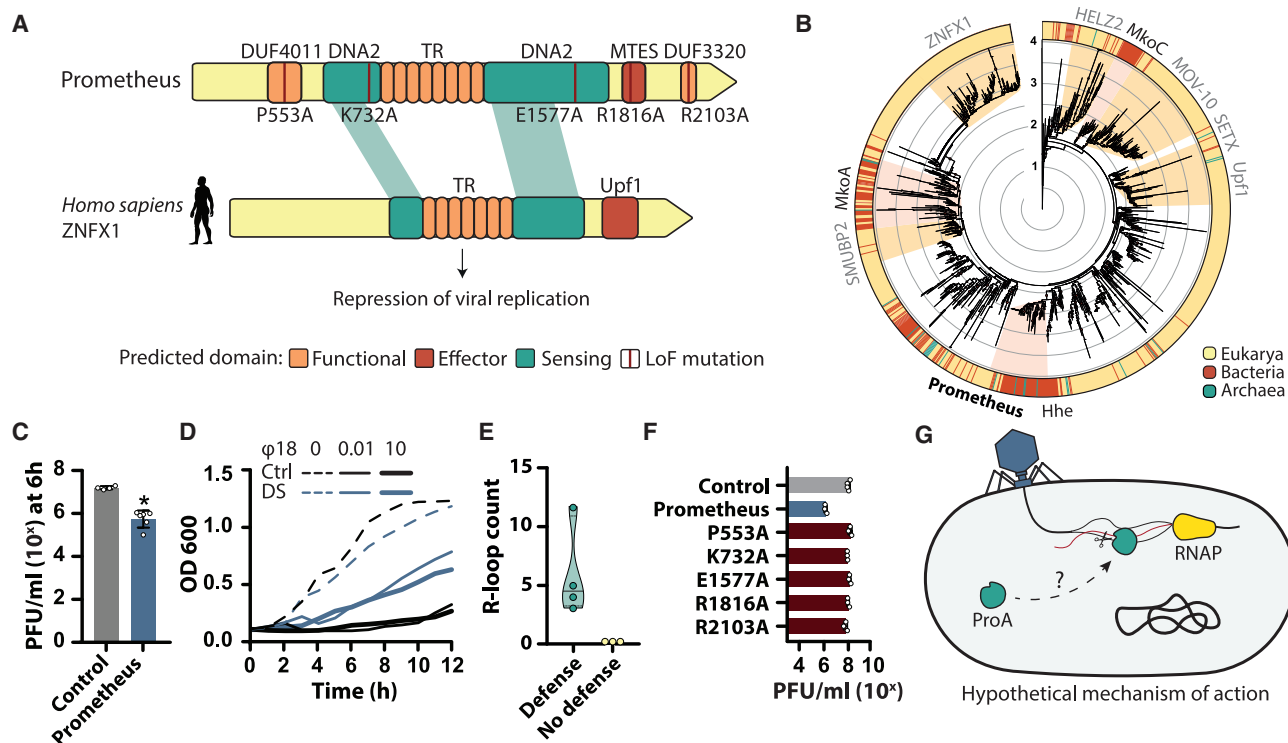


Figure 3. Prometheus is a homolog of a multitude of human DNA2 antiviral defense genes

(A) The functional domains of Prometheus, mutation sites tested in (F), and sequence similarity to the antiviral eukaryotic protein ZNF1 from *Homo sapiens* (NP_066363.1). LoF, loss of function.

(B) Phylogenetic tree of DNA2-containing proteins. The phylogenetic tree of 1,124 representative proteins was inferred and bootstrapped using IQ-Tree2. Branches with a bootstrap confidence interval $\geq 90\%$ are indicated with red dots. The phylogenetic tree was rooted with the ATP-dependent DNA helicase RecG protein (Genbank: NP_254032.1) from *P. aeruginosa* PAO1. The clades of human MOV-10, HELZ2, Upf1, ZNF1, SETX, and SMUBP-2, prokaryotic Prometheus ProA, and DNA2-containing phage defense systems hhe and Mokosh type I/II (MkoA and MkoC) are indicated in the tree.

(C) Impact of Prometheus on phage propagation in liquid culture. The propagation of phage ϕ Pa18 was monitored over time, and the 6 h time point is shown here, with all data points displayed in Figure S2B. The control bar represents phage propagation in PAO1 containing an empty plasmid. Bars represent the average of six biological replicates with individual points and standard deviation shown. * p < 0.05.

(D) Effect of the defense system on bacterial growth upon phage infection. PAO1 cells containing an empty plasmid (control) or Prometheus (defense system [DS]) were infected with phage ϕ Pa18 at low (0.01) and high (10) multiplicity of infection, and their growth was monitored for a period of 12 h. Curves represent the average of three biological replicates.

(E) A violin plot comparing the number of predicted R-loops in targeted and non-targeted phages.

(F) Effect of mutations in the functional domains of Prometheus on phage protection. The concentration of phage ϕ Pa18 when spotted on PAO1 cells containing an empty plasmid (control), Prometheus, or Prometheus with LoF point mutations, as assessed by plaque assay. Bars represent the average of at least three biological replicates with individual points and standard deviation shown.

(G) Prometheus is hypothesized to interfere with phage nucleic acids during transcription.

share a DNA2 and (ribo)nuclease domain with Prometheus and provide protection against various viruses, such as Epstein-Bar virus, Influenza, West Nile virus, and human immunodeficiency virus 1 (HIV-1).^{21,25–32} Interestingly, in both Prometheus and its eukaryotic homologs, the DNA2 domain is split into two parts by tandem repeats, although the function of this arrangement is unknown (Figure 3A). The antiviral human homologs of Prometheus regulate viral transcription through an R-loop dependent mechanism. Targeting of these RNA-DNA hybrids with a dis-

placed single-stranded DNA (ssDNA) strand,⁵⁸ which are formed during transcription,⁵⁹ often results in transcription termination or attenuation.⁶⁰

We hypothesized that Prometheus exerts its antiviral response by interfering with phage transcripts through action on R-loops formed during transcription. Testing this hypothesis, we observed that Prometheus provides protection against podophages ϕ Pa3 and ϕ Pa18 from the *Autographiviridae* family, siphophage ϕ Pa28 from the *Casadabanvirus* genus, and siphophage

(I) Adsorption of phage to LPS extracts containing also capsular polysaccharides (CPSs) from cells carrying an empty plasmid (control), Hermes, or Hermes with an LoF point mutation (D89A). The values indicate the average concentration of phage bound to decreasing amounts of C/LPS from each strain, for at least three biological replicates, with standard deviations shown.

(J) Proposed model for anti-phage defense by Hermes (HrsA). Hermes induces changes in the surface structures of *P. aeruginosa*, such as CPS and LPS, leading to the prevention of phage adsorption.

φPa53 from the *Mesyanzhinovviridae* family, as observed in efficiency of plating assays (Figure 1B), liquid cultures (Figures 3C and S2B), and bacterial growth experiments during phage predation (Figure 3D). Interestingly, these phages contain 3–12 transcribed DNA regions prone to R-loop formation,⁶¹ whereas phages unaffected by Prometheus have no predicted R-loops (φPa36, φPa10, and φPa34) (Figures 3E and S2C). We noticed that Prometheus homolog hhe protected against phage lambda with one predicted R-loop and was unable to protect against phages lacking R-loops, such as T2, T4, T5, P1, and M13⁶ (Table S3), while Mokosh can protect more broadly.⁷

We found that mutations of conserved residues in any of the four domains (DUF4011, DNA2, REase MTES, and DUF3320) abrogated protection, indicating that all domains are essential for Prometheus function (Figure 3F). Further investigations using RNA sequencing (RNA-seq) to analyze transcription profiles of phage φPa18 in control versus Prometheus cells revealed a 10-fold decrease in phage overall transcription (Figure S2D). This decrease was also evident in the phage genomic abundance in the presence of Prometheus, suggesting suppression of phage replication (Figure S2D). To understand the suppression of replication, we further looked into the domain organization of Prometheus. The REase MTES domain belongs to the Swt1-like protein family found in several eukaryotic groups.⁶² In eukaryotes, Swt1 proteins act as RNA endonucleases, playing a role in the quality control of nuclear mRNA export, a crucial step in eukaryotic gene expression.⁶³ However, research on a bacterial Prometheus homolog in *Geobacillus stearothermophilus* indicates that the protein functions as a ssDNA endonuclease.⁵⁷ This suggests that Prometheus might act as a ssDNA endonuclease on the displaced ssDNA of the R-loop through the actions of the DNA2 nuclease and/or REase MTES domains. The activity of the DNA2 helicase/nuclease domain may be facilitated by the putative helicase-related domains DUF4011 and DUF3320⁶⁴ (Figure 3F). Notably, DUF3320 is absent in 54% of instances of Prometheus, even though mutagenesis of this domain (as well as of DUF4011) results in inactivation of the system (Figure 3F). Structural predictions indicate that the DUF3320 domain in Prometheus is similar to a DNA-binding fork head domain (Figure S2E; DALI Z score: 6.3), suggesting a potential role in facilitating the helicase or R-loop binding of DNA2 in Prometheus.

In summary, our analysis highlights Prometheus as a defense system with similarities to eukaryotic antiviral proteins containing DNA2 helicase/nuclease domains. This resemblance suggests a shared mechanism for countering viral infections by acting on viral R-loop structures formed during transcription (hypothetical model proposed in Figure 3G).

Erebus and Hypnos contain NACHT domains

bNACHT Erebus and bNACHT Hypnos are named after the Greek god personification of darkness (Erebus) and his nephew Hypnos, the Greek god of sleep. Both anti-phage systems show similarities with eukaryotic antiviral inflammasome components, representing NACHT domain-containing NLR proteins (nucleotide-binding domain leucine-rich repeat containing, also known as nucleotide oligomerization domain (NOD)-like receptors). NLRs are part of the STAND superfamily and function in antiviral activities within almost all domains of life⁶⁵ (Figure 4A; Table 1). Of these eukaryotic NLRs, Erebus and Hypnos are most similar

to intracellular-pathogen NLR family caspase recruitment domain (CARD)-containing protein 4 (NLRC4). NLRC4 contains several functional domains, including NACHT, an N-terminal CARD, and a C-terminal leucine-rich repeat (LRR).⁶⁶ Erebus and Hypnos share common features with NLRC4 such as the presence of the NACHT domain, but also a protein repeat structure: the tetratricopeptide repeat (TPR) domain. In addition, Erebus and Hypnos contain DNA-acting functional domains not previously associated with phage defense, instead of the CARD domain in NLRC4.

Hypnos and Erebus provide robust protection against myophages φPa10 and φPa34 from the *Pbunavirus* genus (Erebus) and podophages φPa3 and φPa18 from the *Autographiviridae* family (Hypnos), resulting in a reduction of phage infectivity by at least 10⁴-fold in efficiency of plating assays (Figure 1B). Both defense systems limit phage propagation (φPa34 by Erebus, φPa18 by Hypnos) in liquid culture (Figures 4B and S3A). While Erebus allows full recovery of bacterial growth during phage infection (Figure 4C), Hypnos provides a benefit in bacterial growth approximately 2 h post-infection (Figure 4C). Point mutations of conserved amino acids in the NACHT Walker A ATP binding pocket of both defense systems (K50A in Erebus and K52A in Hypnos) resulted in the complete loss of phage protection (Figure 4D).

In humans, plants, and fungi, NACHT-containing NLRs are widely involved in the recruitment of the inflammasome during the innate immune response upon sensing pathogen-derived biomolecules.⁶⁸ Although some NACHT-containing NLRs are found to be activated upon sensing viral dsRNA,⁶⁹ the vast majority sense pathogen-derived proteins.^{70–72} Recently, some clades of prokaryotic NACHT domain containing NLRs have been found to provide phage defense.⁶⁷ Here, we demonstrate anti-phage activity by NACHT proteins from clade 20 (Figure 4E), Erebus, and Hypnos, characterized by an N-terminal NACHT domain, a central TPR domain, and effector domains NucS and SfsA-N at their C terminus (Figures 4A and 4F). This organization is distinct from most NACHT domain-containing NLRs, which typically display an N-terminal effector instead.⁶⁷ Moreover, Erebus and Hypnos encode two TPR regions linked by a helical bridge (Figure 4F), and mutagenesis of this bridge resulted in the loss of phage defense (R740A in Erebus and R817A in Hypnos, Figure 4D).

In other NACHT-like defense systems, the NACHT-like domain physically associates with the effector domain to prevent its activity. This inhibition is lost upon TPR-mediated sensing of phage infection, resulting in protein multimerization,⁶⁵ and activation of the effector domain. In line with these observations, the effector domains of both Erebus and Hypnos are structurally predicted to be near the NACHT domain, suggesting that the NACHT domain may prevent the activity of the effector domain until the target is sensed, similar to the role of NACHT in eukaryotes⁷² (Figures 4F, S3B, and S3C). It remains unclear if multimerization is required for the activation of the effector domains,^{73,74} since these domains and this unusual domain organization has not been characterized before. However, the effector domain of Erebus, NucS, is known for binding and cleaving ssDNA extremities of branched DNA,⁷⁵ while the oligonucleotide/oligosaccharide-binding (OB) fold of SfsA-N in Hypnos likely provides non-specific DNA-binding or cleaving capabilities.^{74,76}

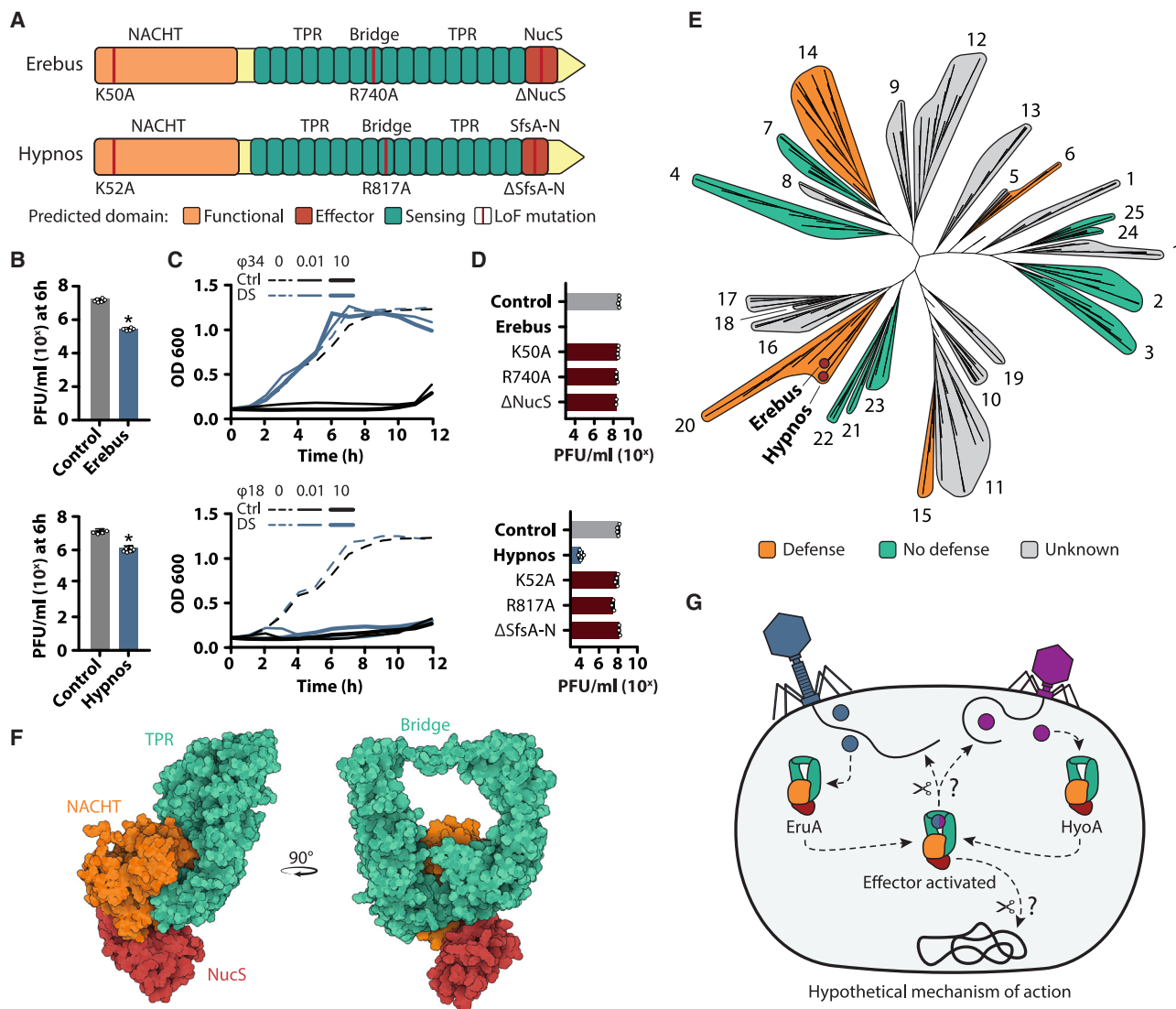


Figure 4. Erebus and Hypnos are NACHT-containing anti-phage NLRs with strong homology to eukaryotic antiviral NLRs

(A) The functional domains of Erebus and Hypnos and mutation sites tested in (D). LoF, loss of function.

(B) Impact of Erebus and Hypnos on phage propagation in liquid culture. The propagation of phage ϕ Pa34 for Erebus and ϕ Pa18 for Hypnos was monitored over time, and the 6 h time point is shown here, with all data points displayed in Figure S3A. The control bar represents phage propagation in PAO1 containing an empty plasmid. Bars represent the average of at least four biological replicates with individual points and standard deviation shown. * $p < 0.05$.

(C) Effect of Erebus (top) or Hypnos (bottom) on bacterial growth upon phage infection. PAO1 cells containing an empty plasmid (control) or the defense system (DS) were infected with phage ϕ Pa34 for Erebus and ϕ Pa18 for Hypnos at low (0.01) and high (10) multiplicity of infection, and their growth was monitored for a period of 12 h. Curves represent the average of three biological replicates.

(D) Effect of mutations in the functional domains of Erebus and Hypnos on phage protection. The infectivity of phage ϕ Pa34 for Erebus and ϕ Pa18 for Hypnos on PAO1 cells containing an empty plasmid (control), defense system, or defense system with point mutations was measured by plaque assay. Bars represent the average of at least three biological replicates with individual points and standard deviation shown.

(E) Phylogenetic tree of all bacterial NACHT domain containing NLRs. The phylogenetic tree was built from the proteins provided by Kibby et al.⁶⁷ ($n = 3,247$) and inferred using FastTree. The clades are colored based on their antiviral properties.

(F) Tertiary structure of Erebus predicted by AlphaFold2. The functional domains are color-coded, with TPR shown in green, NACHT in orange, and the effector domain (NucS) in red.

(G) Hypothetical model for anti-phage defense by Erebus (EruA) and Hypnos (HyoA), with only Erebus shown. Erebus and Hypnos are hypothesized to sense phage infection using the TPR domains, causing a conformational change in the NACHT domain that leads to the release of the effector domain. The effector domains will likely initiate the antiviral response via DNA-acting mechanisms.

Collectively, our findings reveal the anti-phage activity of two NACHT-containing NLR proteins, Erebus and Hypnos, with strong similarity to eukaryotic NACHT-containing antiviral pro-

teins. Based on this similarity, we propose that upon sensing the presence of phage proteins by the bridge-linked TPR domains, the NACHT domain undergoes a conformational change,

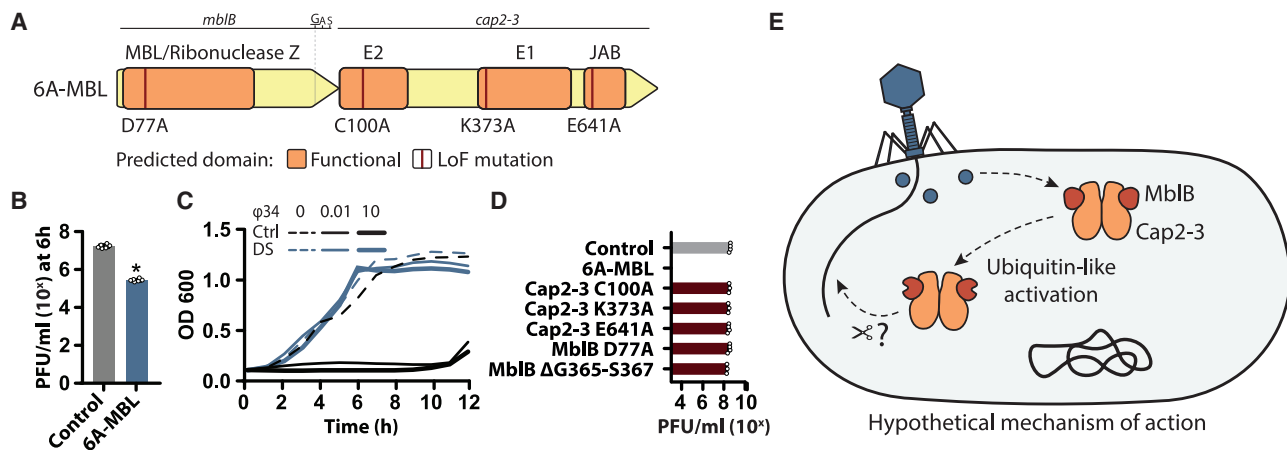


Figure 5. 6A-MBL employs a ubiquitination-like mechanism to activate an MBL-fold protein

(A) The functional domains of 6A-MBL and mutation sites tested in (D). LoF, loss of function. The location of a conserved glycine (G) at the C-terminal of the MBL is indicated above the gene and represents the residue where the substrate protein is commonly linked to its target via a ubiquitin-like mechanism. (B) Impact of 6A-MBL on phage propagation in liquid culture. The propagation of phage ϕ Pa34 was monitored over time, and the 6 h time point is shown here, with all data points displayed in Figure S4A. The control bar represents phage propagation in PAO1 containing an empty plasmid. Bars represent the average of six biological replicates with individual points and standard deviation shown. * $p < 0.05$. (C) Effect of the defense system on bacterial growth upon phage infection. PAO1 cells containing an empty plasmid (control) or 6A-MBL (defense system [DS]) were infected with phage ϕ Pa34 at low (0.01) and high (10) multiplicity of infection, and their growth was monitored for a period of 12 h. Curves represent the average of three biological replicates. (D) Effect of mutations in the functional domains of 6A-MBL on phage protection. The infectivity of phage ϕ Pa34 on PAO1 cells containing an empty plasmid (control), 6A-MBL, or 6A-MBL with point mutations was assessed by plaque assay. Bars represent the average of at least three biological replicates with individual points and standard deviation shown. (E) Hypothetical model for anti-phage defense by 6A-MBL. 6A-MBL is hypothesized to sense phage infection through the fused E1-E2-JAB protein (Cap2-3), leading to the activation of a potential nuclease activity of the MBL-fold protein (MblB).

activating the effector domain (NucS or SfsA-N) and triggering the initiation of the antiviral response, possibly through DNA cleaving or DNA repressing mechanisms (hypothetical model proposed in Figure 4G).

6A-MBL contains a ubiquitination-like domain and an MBL-fold protein

6A-MBL contains one gene with a fused E1-E2-JAB functional domain (Cap2-3) and a second gene with an MBL-fold functional domain (MblB)⁷⁷ (Figure 5A; Table 1). In eukaryotes, E1, E2, and JAB (DUB) function in the ubiquitin signaling pathway, which fine-tunes the eukaryotic innate immunity by either modulating the stability of key molecules or by regulating cytokine production.⁷⁸ In bacteria, these functional domains provide phage defense in cyclic-oligonucleotide-based anti-phage signalling systems (CBASS) type II via a ubiquitin-like mechanism termed cGASylation.⁷⁹ The E1-E2 Cap2 protein of CBASS type II is responsible for cGAS conjugation of CD-NTase to a target molecule upon viral infection. JAB Cap3 functions as a regulator of cGASylation by cleaving the cGAS conjugates.⁷⁹ Previously identified phage defense systems had E1-E2 and JAB encoded by separate genes,^{7,79} but in 6A-MBL these are fused. Here, we show that this configuration provides strong protection against myophages ϕ Pa10 and ϕ Pa34 of the *Pbunavirus* genus and jumbo myophage ϕ Pa36 of the *Phikzvirus* genus, resulting in a reduction of phage infectivity by at least 10⁴-fold in efficiency of plating assays (Figure 1B). 6A-MBL limits the propagation of phage ϕ Pa34 in liquid cultures (Figures 5B and S4A) and allows full recovery of bacterial growth during phage infection (Fig-

ure 5C). Point mutations in conserved amino acids of each predicted functional domain resulted in the complete loss of phage protection (Figure 5D).

Based on previous studies on E1-E2 and JAB components of antiviral responses in both eukaryotes and prokaryotes,^{78,79} we hypothesize that upon phage infection, the E1-E2 and JAB domains of 6A-MBL prime the MBL-fold protein for activation through a ubiquitin-like mechanism. This may be aided by complex formation between the two proteins, as predicted by AlphaFold. The complex consists of a dimer of Cap2-3 connected by the E1 domains. The E2 and JAB domains of Cap2-3 interact with MblB, forming a heterodimeric complex (Figure S4B). In addition, we observed a conserved glycine (G395) in the C-terminal region of MblB in proximity of the active site of the JAB domain of Cap2-3⁷⁹ (Figure 5A). These conserved glycine residues at the C-terminal region often serve as the conjugation site in other ubiquitin-like phage defense systems, such as CBASS type II.^{79–82} In CBASS type II, conjugation of the cyclase to its target increases signal molecule production activating downstream anti-phage effectors. Here, we suspect MblB to go through a similar activation step, and this is supported by the loss of protection observed when deleting G395-A396-S397 in MblB (Figure 5D). However, the mechanism of this activation remains unclear. The MBL-fold was originally discovered in beta-lactamases and later found to be widely distributed in various proteins, exhibiting hydrolase activity targeting nucleic acids and small molecules.⁸³ The MBL-fold protein of 6A-MBL shows strong structural similarity to the OB-fold domain of DNA internalization-related competence protein ComEC

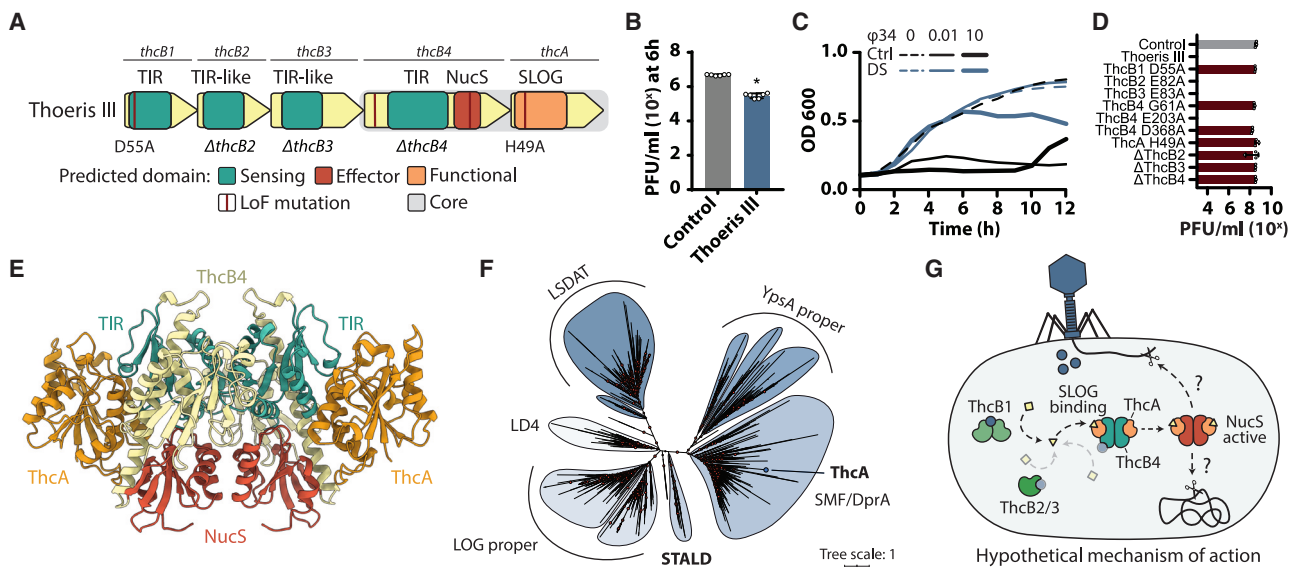


Figure 6. Thoiris type III is a phage defense system of the TIR domain antiviral family

(A) The functional domains of Thoiris III and mutation sites tested in (D).

(B) Impact of Thoiris type III on phage propagation in liquid culture. The propagation of phage ϕ Pa34 was monitored over time, and the 6 h time point is shown here, with all data points displayed in Figure S5A. The control bar represents phage propagation in PAO1 containing an empty plasmid. Bars represent the average of six biological replicates with individual points and standard deviation shown. * $p < 0.05$.

(C) Effect of Thoiris type III on bacterial growth upon phage infection. PAO1 cells containing an empty plasmid (control) or Thoiris type III (defense system [DS]) were infected with phage ϕ Pa34 at low (0.01) and high (10) multiplicity of infection, and their growth was monitored for a period of 12 h. Curves represent the average of three biological replicates.

(D) Effect of gene deletions and mutations in the functional domains of Thoiris type III on phage protection. The infectivity of phage ϕ Pa34 on PAO1 cells containing an empty plasmid (control), Thoiris type III, or Thoiris type III with point mutations was assessed by plaque assay. Bars represent the average of at least three biological replicates with individual points and standard deviation shown.

(E) Tertiary structure of the ThcA:ThcB4 tetramer predicted by AlphaFold2. The SLOG-containing ThcA is shown in orange, and the TIR and NucS domains of ThcB4 are shown in green and red, respectively.

(F) Phylogenetic tree of SLOG-containing proteins. The phylogenetic tree of 13,399 representative proteins was inferred and bootstrapped using IQ-Tree2. The representative proteins include all groups within the SLOG clan (CL0349), as indicated in the tree. Branches with bootstrap confidence interval $\geq 90\%$ are indicated with red dots.

(G) Hypothetical model for anti-phage defense by Thoiris type III. Thoiris type III is hypothesized to sense phage infection by TIR proteins (ThcB1 for ϕ Pa34), leading to the production of signaling molecules. These are likely detected by the SLOG domain of ThcA for the activation of the NucS endonuclease effector response by ThcB4, with which it forms a complex.

(Foldseek⁸⁴ E value: $1.56e-11$), a protein predicted to be a nuclease.⁸⁵ It is therefore possible that the MBL-fold protein of 6A-MBL acts as the nucleic acid acting effector upon phage infection.

In summary, our findings demonstrate that 6A-MBL is an anti-phage defense system with similarities to eukaryotic antiviral proteins associated with the ubiquitin pathway and CBASS type II. Based on this similarity, we hypothesize that 6A-MBL senses phage infection by the fused E1-E2-JAB protein (Cap2-3), which may use a ubiquitin-like pathway to activate the MBL-fold protein (MblB), resulting in anti-phage activity (hypothetical model proposed in Figure 5E).

Thoiris type III expands the TIR domain antiviral family

Thoiris type III contains a SLOG domain protein (ThcA) accompanied by four TIR(-like) domain-containing proteins (ThcB1–B4) (Figure 6A; Table 1). ThcA and ThcB4 are consistently encoded within the Thoiris type III cluster, while the remaining genes exhibit variable presence (ThcB1: 51%; ThcB2 and ThcB3 combined: 18%; either ThcB2 or ThcB3: 64%), establishing them as

core genes of this defense system. Thoiris type III exhibits robust protection against a myophage from the *Pbunavirus* genus (ϕ Pa34), reducing its infectivity by more than 10^6 -fold in efficiency of plating assays (Figure 1B). It efficiently reduces phage proliferation in liquid cultures (Figures 6B and S5A) and facilitates nearly complete recovery of bacterial growth during phage predation (Figure 6C). Mutations in conserved amino acids within core protein ThcA (SLOG, H49A) and accessory TIR domain containing protein ThcB1 (TIR, D55A) resulted in the loss of defense, while mutagenesis of the active site of other TIR proteins (ThcB2 E82A, ThcB3 E83A, ThcB4 E203A) within the cluster did not result in the loss of defense activity (Figure 6D). However, deletion of any TIR domain proteins led to a complete loss of protection, indicating that the presence of all TIR domain proteins is necessary, while all the individual TIR enzymatic activities are not (Figure 6D).

In eukaryotes, TIR domains serve as scaffolding adapters during inflammation, orchestrating pro-inflammatory responses through complex formation involving TIR domains of different proteins.⁸⁶ ThcB4 is homologous to one such eukaryotic

scaffolding TIR domain-containing protein, SARM1 (Table 1). However, unlike SARM1, ThcB4 lacks obvious multimerization (sterile alpha motif, SAM) and autoinhibition (armadillo, ARM) domains that regulate TIR domain activity.^{87,88} Eukaryotic TIR domains also serve to signal pathogen recognition by protein repeats of the Toll-like receptors.⁸⁹ In bacteria, the TIR domains of the Thoreris defense family signal defense effectors upon sensing phage infection. Unlike eukaryotic Toll-like receptors, Thoreris TIR domains function both as scaffolding proteins and phage sensors, independently of protein repeat structures that function as the main pathogen sensors in eukaryotes.¹³ In Thoreris types I and II, TIR proteins sense phage infection, generating secondary messenger molecules (cyclic ADP-ribose [cADPR] or histidine-ADPR, respectively).⁹⁰ These molecules are recognized by the SLOG(-like) domain, which activates the effector present on the same protein, leading to phage defense.

In Thoreris type III, the two core proteins, ThcB4 and ThcA, are predicted to form a tetrameric complex of two heterodimer subunits of ThcB4 and ThcA (Figures 6E, S5B, and S5C). In this configuration, the NucS endonuclease domain of ThcB4 is in direct contact with the SLOG domain of ThcA, indicating a potential regulatory role of SLOG. This observation aligns with previous characterizations of Thoreris types, where SLOG substrate binding physically activates the effector domain.⁹⁰ Unlike previous Thoreris types, the SLOG domain of Thoreris type III belongs to the LD_cluster_3 clade of the SMF/DprA SLOG superfamily, distinct from the traditional SIR2/TIR-associated SLOG domains (STALD) (Figure 6F). Moreover, the SLOG domain of Thoreris type III is also predicted to establish direct contact with the TIR domain of ThcB4 (Figure 6E), likely facilitating TIR domain signaling to the SLOG domain upon phage infection sensing. However, mutagenesis of the TIR domain of ThcB4 (E203A) did not result in defense loss (Figure 6D), suggesting the production of signaling molecules may be assumed by other TIR domain proteins within Thoreris type III. For ϕ Pa34, this role appears to be carried out by the TIR domain of accessory protein ThcB1, as mutation of its active site (D55A) resulted in defense loss (Figure 6D). Based on the requirement of ThcB2 and ThcB3 but not their TIR activity for full system functioning (Figure 6D), we expect these to be sensors of phages outside our panel. Mutagenesis of a conserved residue (G61A) in the Rossmann fold of ThcB4, predicted to bind reduced nicotinamide adenine dinucleotide (NADH) and to be essential for TIR activity, resulted in complete loss of protection, indicating that the activity of ThcB4 is also necessary for Thoreris defense (Figure 6D).

Interestingly, the TIR domain of ThcB1, which is required for the defense against ϕ Pa34, is phylogenetically distinct from previously described TIR domains of Thoreris and structurally resembles the dimeric Cap12 TIR domain present in effectors of the CBASS and Pycsar defense systems⁹¹ (Figures S5C–S5E). Unlike these systems where the Cap12 TIR domain causes cellular NAD⁺ depletion upon phage infection, no change was observed in cellular NAD⁺ levels during phage infection in Thoreris type III, suggesting that ThcB1 likely acts as a phage sensor rather than an NAD⁺ depleting effector (Figure S5F).

Here, the TIR domains in Thoreris type III likely produce ADPR derivatives upon phage sensing, similar to Thoreris type I and II systems, to signal the SLOG domain of ThcA for activating the

NucS endonuclease domain of core protein ThcB4. Mutagenesis of a conserved amino acid (D368A) in the NucS domain resulted in loss of defense, further supporting a crucial role of the NucS domain, likely as an anti-phage effector nuclease (Figure 6D).

In summary, Thoreris type III represents an addition to the anti-viral TIR domain family, which carries a distinct Thoreris-associated class of SLOG domain that likely activates the anti-phage NucS nuclease effector in ThcB4 (hypothetical model proposed in Figure 6G).

Distribution of the anti-phage repertoire across bacterial phyla

Analysis of the distribution of the defense systems in prokaryotic genomes revealed that Prometheus and 6A-MBL are the most widely distributed systems (Table S4; Figure S6). Prometheus was found in seven bacterial phyla, exhibiting the highest abundance in Actinomycetota (Figures S2F and S2G), while 6A-MBL was found in eleven bacterial phyla, predominantly prevalent within Proteobacteria (Figures S4C and S4D). The remaining four defense systems were almost exclusively (>92%) observed in Proteobacteria, spanning various classes, except for Hermes, which is restricted to Gammaproteobacteria (Figures S1G, S1H, S3D, S3E, S5G, and S5H; Table S4).

To assess the impact of the defense systems on the diverse and abundant defense repertoire in *P. aeruginosa*,^{10,20} we determined their distribution across all complete genomes ($n = 541$) available from the RefSeq database. Prometheus and 6A-MBL are well distributed across the *P. aeruginosa* groups (Figures S2H and S4E; Table S5). Hermes, Erebus, Hypnos, and Thoreris III are less abundant in *P. aeruginosa* (Figures S1I, S3F, and S5I; Table S5). Collectively, the six validated systems constitute 3% of the total defense systems found in *P. aeruginosa* and increase the average number of defense systems per strain from 9.7 to 10.0 (Table S5). All new defense systems can often be found within close proximity of known defense systems (Figures 1A, S1J, S2I, S3G, S4F, and S5J).^{4,8} In summary, the defense systems described here have a prominent presence among Proteobacteria and contribute to the phage defense repertoire of *P. aeruginosa*.

DISCUSSION

In this study, we searched for bacterial homologs of eukaryotic antiviral defense genes in *P. aeruginosa* with antiphage properties. We uncovered more than 450 candidates located in proximity to known anti-phage defenses. Experimental testing of eleven candidates revealed six eukaryotic-like anti-phage defenses, including Hermes, Prometheus, Erebus, Hypnos, 6A-MBL, and Thoreris III. Five candidate defense systems eluded experimental validation, possibly due to the limited panel of phages, the presence of unknown phage-encoded anti-genes, or incompatibility with the genetic background in the *P. aeruginosa* test strain. Of the ones that were validated, Hermes features a eukaryotic-like antiviral functional domain not previously associated with anti-phage activities in bacteria. This defense system causes alterations in surface structures crucial for phage receptor interactions, effectively preventing phage adsorption, akin to the antiviral function of its eukaryotic homologs.⁵¹ Likewise, Prometheus is thought to play a role analogous to its eukaryotic counterparts.^{59,60}

We also report the eukaryotic-like defense systems bNACHT Erebus, bNACHT Hypnos, 6A-MBL, and Thoeris III, each potentially equipped with nucleic acid interfering activities. Among these, Erebus and Hypnos represent anti-phage NACHT-containing NLR proteins from NACHT clade 20, which display a domain architecture distinct from most NACHT-containing NLRs,⁶⁷ characterized by an N-terminal NACHT domain, central TPR domain, and C-terminal effector. This is an indication that the antiviral function of NACHT-containing NLRs is independent of domain organization and conserved across almost all domains of life.⁶⁵ Furthermore, while the precise phage sensing mechanisms of these systems remain enigmatic, the presence of TPR domains in Erebus and Hypnos suggests a potential interaction with specific phage proteins as their targets.

Another interesting finding is an anti-phage E1-E2-JAB fusion in the 6A-MBL system. Previously, these domains were described in unfused proteins, found both in eukaryotes and prokaryotes, where they participate in ubiquitin-like signaling pathways crucial for modulating innate immunity.^{41,78,91} In the prokaryotic defense systems CBASS and Pycsar, these proteins prime bacterial cyclases for increased production of signaling molecules, which subsequently activate an effector.⁷⁹ In the context of 6A-MBL, it seems likely that the E1-E2-JAB fusion protein regulates the activity of an MBL protein through a ubiquitin-like mechanism that regulates its anti-phage activity.

Finally, Thoeris III represents a member of the TIR domain antiviral family found across eukaryotes and prokaryotes. Comprising several TIR domain-containing accessory proteins (ThcB1, ThcB2, and ThcB3) and two core proteins (ThcB4 and ThcA), Thoeris type III is distinct from other Thoeris types by employing a unique class of SLOG, an endonuclease as a putative effector, and encoding the effector and SLOG domains in unfused proteins that form a tetrameric complex.³⁹ It is noteworthy that the endonuclease NucS present in Thoeris type III is an endonuclease effector domain not previously linked to anti-phage defense and is also found in bNACHT Erebus.

Four out of six of the validated defense systems in our study share domains with recently reported phage defense systems in bacteria.^{41,67,91} This phenomenon underscores the remarkable shared nature of anti-phage protein domains to other genetic contexts, which underlies the rapid diversification in host-pathogen interactions and evolution of innovative functions.⁹² This observation is relevant due to its potential to accelerate the mechanistic characterization of these defense systems. Currently, the pace of understanding the workings of defense mechanisms significantly lags the discovery of new systems.^{93–96} Shared domains among these systems offer a promising bridge to narrow this knowledge gap. By leveraging insights gained from the study of one system to better comprehend another, we can expedite our understanding of the molecular intricacies that drive these defense mechanisms.

The discovery that multiple defensive proteins employed by human cells possess direct homologs in prokaryotes, functioning in viral defense, illuminates the cross-domain links in the evolution of the human defense system and holds implications for future mechanistic studies of human innate immunity. By expanding our knowledge of eukaryotic-like phage defenses, we can gain further insights into these perspectives. The comprehensive exploration and characterization of prokaryotic

antiviral defenses could yield a plethora of new biotechnological, therapeutic, and diagnostic tools, as seen previously with restriction-modification systems, CRISPR-Cas and Argonaute, which have led to widespread methods for DNA and RNA engineering.^{97–103}

Altogether, we show the existence of antiviral pathways that are shared between bacteria and eukaryotes. Detailed future studies will be required to unveil the molecular mechanisms of these defense systems, and this will further help to understand the complex relationship between host defense mechanisms of different domains of life that are potentially forged through a shared viral past.

STAR★METHODS

Detailed methods are provided in the online version of this paper and include the following:

- KEY RESOURCES TABLE
- RESOURCE AVAILABILITY
 - Lead contact
 - Materials availability
 - Data and code availability
- EXPERIMENTAL MODEL AND SUBJECT DETAILS
 - Bacteria and phages
- METHOD DETAILS
 - Identification of anti-phage defense systems
 - Identification of conserved gene clusters within the variable regions of *Pseudomonas aeruginosa*
 - Cloning of the putative eukaryotic-like defense systems
 - Selection for point mutations
 - Cloning of knockout and point mutants of the defense systems
 - Efficiency of plating
 - Infection dynamics of phage-infected cultures
 - Liquid culture collapse assays
 - Screening for mutant phages that escape defense
 - LC-MS analysis
 - Phage adsorption kinetics in Hermes
 - Extraction and visualization of outer membrane protein
 - Extraction and visualization of lipopolysaccharides
 - Extraction and visualization of capsule density
 - Phage adsorption to capsule and lipopolysaccharides
 - Protein complex prediction
 - Phage R-loop prediction
 - Comparison of IMPA, SuhB, and HrsA
 - RNA-seq experiments with Prometheus
 - Sequencing during phage infection
 - NAD/NADH measurements
 - Building HMM models of the defense systems
 - Search for novel defense systems in archaeal and bacterial genomes
 - Phylogenetic tree and annotation of the defense system genes
 - Phylogeny tree of *Pseudomonas aeruginosa*
- QUANTIFICATION AND STATISTICAL ANALYSIS

SUPPLEMENTAL INFORMATION

Supplemental information can be found online at <https://doi.org/10.1016/j.chom.2024.07.007>.

ACKNOWLEDGMENTS

We thank the Delft University of Technology and the University of Amsterdam (Swammerdam Institute for Life Sciences, MAD/RB&AB) for the use of the DelftBlue and Crunchomics compute cluster, respectively. This work was supported by grants from the European Research Council (ERC) CoG under the

European Union's Horizon 2020 research and innovation program (grant agreement no. 101003229) and the Netherlands Organisation for Scientific Research (NWO VICI; VI.C.192.027) to S.J.J.B. We also thank members of the Brouns lab for the many discussions and ideas that improved our work.

AUTHOR CONTRIBUTIONS

Conceptualization, S.J.J.B., and D.F.v.d.B.; methodology; S.J.J.B., D.F.v.d.B., and A.R.C.; software, D.F.v.d.B., I.S., and J.Q.G.; formal analysis, D.F.v.d.B., A.R.C., J.Q.E., I.S., and J.Q.G.; investigation, A.R.C., D.F.v.d.B., J.Q.E., and A.D.Z.-D.; visualization, D.F.v.d.B., A.R.C., and J.Q.E.; data curation, A.R.C., D.F.v.d.B., J.Q.E., I.S., and J.Q.G.; writing – original draft, D.F.v.d.B., A.R.C., and J.Q.E.; writing – review & editing, S.J.J.B.; resources: P.J.-H.; funding acquisition, S.J.J.B.

DECLARATION OF INTERESTS

The authors declare no competing interests.

Received: December 4, 2023

Revised: May 21, 2024

Accepted: July 9, 2024

Published: August 1, 2024

REFERENCES

- Hampton, H.G., Watson, B.N.J., and Fineran, P.C. (2020). The arms race between bacteria and their phage foes. *Nature* 577, 327–336. <https://doi.org/10.1038/s41586-019-1894-8>.
- Srikant, S., Guegler, C.K., and Laub, M.T. (2022). The evolution of a counter-defense mechanism in a virus constrains its host range. *eLife* 11, e79549. <https://doi.org/10.7554/eLife.79549>.
- Hussain, F.A., Dubert, J., Elsherbini, J., Murphy, M., VanInsberghe, D., Arevalo, P., Kauffman, K., Rodino-Janeiro, B.K., Gavin, H., Gomez, A., et al. (2021). Rapid evolutionary turnover of mobile genetic elements drives bacterial resistance to phages. *Science* 374, 488–492. <https://doi.org/10.1126/science.abb1083>.
- Hochhauser, D., Millman, A., and Sorek, R. (2023). The defense island repertoire of the *Escherichia coli* pan-genome. *PLoS Genet.* 19, e1010694. <https://doi.org/10.1371/journal.pgen.1010694>.
- Doron, S., Melamed, S., Ofir, G., Leavitt, A., Lopatina, A., Keren, M., Amitai, G., and Sorek, R. (2018). Systematic discovery of antiphage defense systems in the microbial pangenome. *Science* 359, eaar4120. <https://doi.org/10.1126/science.aar4120>.
- Gao, L., Altae-Tran, H., Böhnning, F., Makarova, K.S., Segel, M., Schmid-Burgk, J.L., Koob, J., Wolf, Y.I., Koonin, E.V., and Zhang, F. (2020). Diverse enzymatic activities mediate antiviral immunity in prokaryotes. *Science* 369, 1077–1084. <https://doi.org/10.1126/science.aba0372>.
- Millman, A., Melamed, S., Leavitt, A., Doron, S., Bernheim, A., Hör, J., Garb, J., Bechon, N., Brandis, A., Lopatina, A., et al. (2022). An expanded arsenal of immune systems that protect bacteria from phages. *Cell Host Microbe* 30, 1556–1569.e5. <https://doi.org/10.1016/j.chom.2022.09.017>.
- Johnson, M.C., Laderman, E., Huiting, E., Zhang, C., Davidson, A., and Bondy-Denomy, J. (2023). Core defense hotspots within *Pseudomonas aeruginosa* are a consistent and rich source of anti-phage defense systems. *Nucleic Acids Res.* 51, 4995–5005. <https://doi.org/10.1093/nar/gkad317>.
- Rocha, E.P.C., and Bikard, D. (2022). Microbial defenses against mobile genetic elements and viruses: Who defends whom from what? *PLoS Biol.* 20, e3001514. <https://doi.org/10.1371/journal.pbio.3001514>.
- Costa, A.R., van den Berg, D.F., Esser, J.Q., Muralidharan, A., van den Bossche, H., Bonilla, B.E., van der Steen, B.A., Haagsma, A.C., Fluit, A.C., Nobrega, F.L., et al. (2024). Accumulation of defense systems in phage-resistant strains of *Pseudomonas aeruginosa*. *Sci. Adv.* 10, eadj0341. <https://doi.org/10.1126/sciadv.adj0341>.
- Vassallo, C.N., Doering, C.R., Littlehale, M.L., Teodoro, G.I.C., and Laub, M.T. (2022). A functional selection reveals previously undetected anti-phage defence systems in the *E. coli* pangenome. *Nat. Microbiol.* 7, 1568–1579. <https://doi.org/10.1038/s41564-022-01219-4>.
- Georjon, H., and Bernheim, A. (2023). The highly diverse antiphage defence systems of bacteria. *Nat. Rev. Microbiol.* 21, 686–700. <https://doi.org/10.1038/s41579-023-00934-x>.
- Ka, D., Oh, H., Park, E., Kim, J.-H., and Bae, E. (2020). Structural and functional evidence of bacterial antiphage protection by Thoeris defense system via NAD⁺ degradation. *Nat. Commun.* 11, 2816. <https://doi.org/10.1038/s41467-020-16703-w>.
- Millman, A., Bernheim, A., Stokar-Avihail, A., Fedorenko, T., Voichek, M., Leavitt, A., Oppenheimer-Shaanan, Y., and Sorek, R. (2020). Bacterial Retrons Function In Anti-Phage Defense. *Cell* 183, 1551–1561.e12. <https://doi.org/10.1016/j.cell.2020.09.065>.
- Johnson, A.G., Wein, T., Mayer, M.L., Duncan-Lowey, B., Yirmiya, E., Oppenheimer-Shaanan, Y., Amitai, G., Sorek, R., and Kranzusch, P.J. (2022). Bacterial gasdermins reveal an ancient mechanism of cell death. *Science* 375, 221–225. <https://doi.org/10.1126/science.abc8432>.
- Makarova, K.S., Wolf, Y.I., van der Oost, J., and Koonin, E.V. (2009). Prokaryotic homologs of Argonaute proteins are predicted to function as key components of a novel system of defense against mobile genetic elements. *Biol. Direct* 4, 29. <https://doi.org/10.1186/1745-6150-4-29>.
- Koopal, B., Kruijs, A.J., Claassens, N.J., Nobrega, F.L., and van der Oost, J. (2019). Incorporation of a Synthetic Amino Acid into dCas9 Improves Control of Gene Silencing. *ACS Synth. Biol.* 8, 216–222. <https://doi.org/10.1021/acssynbio.8b00347>.
- Shomar, H., Georjon, H., Feng, Y., Olympio, B., Tesson, F., Cury, J., Wu, F., and Bernheim, A. (2024). Viperin immunity evolved across the tree of life through serial innovations on a conserved scaffold. Published online July 4, 2024. *Nat. Ecol. Evol.* <https://doi.org/10.1101/2023.09.13.557418>.
- Leão, P., Little, M.E., Appler, K.E., Sahaya, D., Aguilar-Pine, E., Currie, K., Finkelstein, I.J., Anda, V.D., and Baker, B.J. (2023). Asgard archaea defense systems and their roles in the origin of immunity in eukaryotes. Preprint at bioRxiv. <https://doi.org/10.1101/2023.09.13.557551>.
- Tesson, F., Hervé, A., Mordret, E., Touchon, M., d'Humières, C., Cury, J., and Bernheim, A. (2022). Systematic and quantitative view of the antiviral arsenal of prokaryotes. *Nat. Commun.* 13, 2561. <https://doi.org/10.1038/s41467-022-30269-9>.
- Miller, M.S., Rialdi, A., Ho, J.S.Y., Tilove, M., Martinez-Gil, L., Moshkina, N.P., Peralta, Z., Noel, J., Melegari, C., Maestre, A.M., et al. (2015). Senataxin suppresses the antiviral transcriptional response and controls viral biogenesis. *Nat. Immunol.* 16, 485–494. <https://doi.org/10.1038/ni.3132>.
- Murphy, A.M., Otto, B., Brearley, C.A., Carr, J.P., and Hanke, D.E. (2008). A role for inositol hexakisphosphate in the maintenance of basal resistance to plant pathogens. *Plant J.* 56, 638–652. <https://doi.org/10.1111/j.1365-3113.2008.03629.x>.
- Bezerra Espinola, M.S., Bertelli, M., Bizzarri, M., Unfer, V., Laganà, A.S., Visconti, B., and Aragona, C. (2021). Inositol and vitamin D may naturally protect human reproduction and women undergoing assisted reproduction from Covid-19 risk. *J. Reprod. Immunol.* 144, 103271. <https://doi.org/10.1016/j.jri.2021.103271>.
- Bizzarri, M., Laganà, A.S., Aragona, D., and Unfer, V. (2020). Inositol and pulmonary function. Could myo-inositol treatment downregulate inflammation and cytokine release syndrome in SARS-CoV-2? *Eur. Rev. Med. Pharmacol. Sci.* 24, 3426–3432. https://doi.org/10.26355/eurrev_202003_20715.
- Zhang, Q., Wang, Y.C., and Montalvo, E.A. (1999). Subp-2 Represses the Epstein-Barr Virus Lytic Switch Promoter. *Virology* 255, 160–170. <https://doi.org/10.1006/viro.1998.9588>.
- Fusco, D.N., Pratt, H., Kandilas, S., Cheon, S.S.Y., Lin, W., Cronkite, D.A., Basavappa, M., Jeffrey, K.L., Anselmo, A., Sadreyev, R., et al. (2017). HELZ2 Is an IFN Effector Mediating Suppression of Dengue

- Virus. *Front. Microbiol.* 8, 240. <https://doi.org/10.3389/fmicb.2017.00240>.
27. Vavassori, S., Chou, J., Faletti, L.E., Haunerding, V., Opitz, L., Joset, P., Fraser, C.J., Prader, S., Gao, X., Schuch, L.A., et al. (2021). Multisystem inflammation and susceptibility to viral infections in human ZNF1 deficiency. *J. Allergy Clin. Immunol.* 148, 381–393. <https://doi.org/10.1016/j.jaci.2021.03.045>.
28. Wang, L., Sola, I., Enjuanes, L., and Zúñiga, S. (2021). MOV10 Helicase Interacts with Coronavirus Nucleocapsid Protein and Has Antiviral Activity. *mBio* 12, e0131621. <https://doi.org/10.1128/mbio.01316-21>.
29. Cuevas, R.A., Ghosh, A., Wallerath, C., Homung, V., Coyne, C.B., and Sarkar, S.N. (2016). MOV10 Provides Antiviral Activity against RNA Viruses by Enhancing RIG-I-MAVS-Independent IFN Induction. *J. Immunol.* 196, 3877–3886. <https://doi.org/10.4049/jimmunol.1501359>.
30. Serquiña, A.K.P., Das, S.R., Popova, E., Ojelabi, O.A., Roy, C.K., and Göttinger, H.G. (2013). UPF1 Is Crucial for the Infectivity of Human Immunodeficiency Virus Type 1 Progeny Virions. *J. Virol.* 87, 8853–8861. <https://doi.org/10.1128/jvi.00925-13>.
31. May, J.P., and Simon, A.E. (2021). Targeting of viral RNAs by Upf1-mediated RNA decay pathways. *Curr. Opin. Virol.* 47, 1–8. <https://doi.org/10.1016/j.coviro.2020.11.002>.
32. Richardson, A., Ponde, N., Ong, S., Khooshemehri, P., Bagley, D., Bucca, G., Hesketh, A., Smith, C., Rosenblatt, J., and Martinez-Nunez, R. (2022). S58 UPF1 is a novel modulator of antiviral responses against rhinovirus and is deficient in patients with severe asthma. *Thorax* 77, A37.3–A3A38. <https://doi.org/10.1136/thorax-2022-BTAbstracts.64>.
33. Breuer, K., Foroushani, A.K., Laird, M.R., Chen, C., Sribnaia, A., Lo, R., Winsor, G.L., Hancock, R.E.W., Brinkman, F.S.L., and Lynn, D.J. (2013). InnateDB: systems biology of innate immunity and beyond—recent updates and continuing curation. *Nucleic Acids Res.* 41, D1228–D1233. <https://doi.org/10.1093/nar/gks1147>.
34. Calle García, J., Guadagno, A., Paytúvi-Gallart, A., Saera-Vila, A., Amoroso, C.G., D'esposito, D., Andolfo, G., Aiese Cigliano, R., Sanseverino, W., and Ercolano, M.R. (2021). PRGdb 4.0: an updated database dedicated to genes involved in plant disease resistance process. *Nucleic Acids Res.* 50, D1483–D1490. <https://doi.org/10.1093/nar/gkab1087>.
35. Richter, D.J., Berney, C., Strasser, J.F.H., Poh, Y.-P., Herman, E.K., Muñoz-Gómez, S.A., Wideman, J.G., Burki, F., and de Vargas, C. (2022). EukProt: A database of genome-scale predicted proteins across the diversity of eukaryotes. *Peer Commun. J.* 2, e56. <https://doi.org/10.24072/pcjournal.173>.
36. Steinegger, M., and Söding, J. (2017). MMseqs2 enables sensitive protein sequence searching for the analysis of massive data sets. *Nat. Biotechnol.* 35, 1026–1028. <https://doi.org/10.1038/nbt.3988>.
37. Zou, J., Chang, M., Nie, P., and Secombes, C.J. (2009). Origin and evolution of the RIG-I like RNA helicase gene family. *BMC Evol. Biol.* 9, 85. <https://doi.org/10.1186/1471-2148-9-85>.
38. Andrisani, O., Liu, Q., Kehn, P., Leitner, W.W., Moon, K., Vazquez-Maldonado, N., Fingerling, I., and Gale, M. (2022). Biological functions of DEAD/DEAH-box RNA helicases in health and disease. *Nat. Immunol.* 23, 354–357. <https://doi.org/10.1038/s41590-022-01149-7>.
39. Ofir, G., Herbst, E., Baroz, M., Cohen, D., Millman, A., Doron, S., Tal, N., Malheiro, D.B.A., Malitsky, S., Amitai, G., et al. (2021). Antiviral activity of bacterial TIR domains via immune signalling molecules. *Nature* 600, 116–120. <https://doi.org/10.1038/s41586-021-04098-7>.
40. Leipe, D.D., Koonin, E.V., and Aravind, L. (2004). STAND, a Class of P-Loop NTPases Including Animal and Plant Regulators of Programmed Cell Death: Multiple, Complex Domain Architectures, Unusual Phyletic Patterns, and Evolution by Horizontal Gene Transfer. *J. Mol. Biol.* 343, 1–28. <https://doi.org/10.1016/j.jmb.2004.08.023>.
41. Millman, A., Melamed, S., Amitai, G., and Sorek, R. (2020). Diversity and classification of cyclic-oligonucleotide-based anti-phage signalling systems. *Nat. Microbiol.* 5, 1608–1615. <https://doi.org/10.1038/s41564-020-0777-y>.
42. Zerbini, F.M., Siddell, S.G., Lefkowitz, E.J., Mushegian, A.R., Adriaenssens, E.M., Alfenas-Zerbini, P., Dempsey, D.M., Dutilh, B.E., García, M.L., Hendrickson, R.C., et al. (2023). Changes to virus taxonomy and the ICTV Statutes ratified by the International Committee on Taxonomy of Viruses (2023). *Arch. Virol.* 168, 175. <https://doi.org/10.1007/s00705-023-05797-4>.
43. Li, K., Xu, C., Jin, Y., Sun, Z., Liu, C., Shi, J., Chen, G., Chen, R., Jin, S., and Wu, W. (2013). SuhB Is a Regulator of Multiple Virulence Genes and Essential for Pathogenesis of *Pseudomonas aeruginosa*. *mBio* 4, e00419-13. <https://doi.org/10.1128/mbio.00419-13>.
44. Holm, L., and Laakso, L.M. (2016). Dali server update. *Nucleic Acids Res.* 44, W351–W355. <https://doi.org/10.1093/nar/gkw357>.
45. Tariq, K., and Luikart, B.W. (2021). Striking a balance: PIP2 and PIP3 signaling in neuronal health and disease. *Explor. Neuroprotective Ther.* 1, 86–100. <https://doi.org/10.37349/ent.2021.00008>.
46. Hu, L., Zhou, K., Ren, G., Yang, S., Liu, Y., Zhang, Z., Li, Y., Gong, X., and Ma, F. (2020). myo-inositol mediates reactive oxygen species-induced programmed cell death via salicylic acid-dependent and ethylene-dependent pathways in apple. *Hortic. Res.* 7, 138. <https://doi.org/10.1038/s41438-020-00357-2>.
47. Goswami, R., Bondoc, J.M.G., Wheeler, P.R., Jafari, A., Gonzalez, T., Mehboob, S., and Movahedzadeh, F. (2018). Inositol Monophosphatase: A Bifunctional Enzyme in *Mycobacterium smegmatis*. *ACS Omega* 3, 13876–13881. <https://doi.org/10.1021/acsomega.8b01753>.
48. Lu, S., Huang, W., Li, X., Huang, Z., Liu, X., Chen, Y., Shi, T., and Zhang, J. (2012). Insights into the Role of Magnesium Triad in myo-Inositol Monophosphatase: Metal Mechanism, Substrate Binding, and Lithium Therapy. *J. Chem. Inf. Model.* 52, 2398–2409. <https://doi.org/10.1021/ci300172r>.
49. Ferruz, N., Tresadern, G., Pineda-Lucena, A., and De Fabritiis, G. (2016). Multibody cofactor and substrate molecular recognition in the myo-inositol monophosphatase enzyme. *Sci. Rep.* 6, 30275. <https://doi.org/10.1038/srep30275>.
50. Faisal Tarique, K., Arif Abdul Rehman, S., and Gourinath, S. (2014). Structural elucidation of a dual-activity PAP phosphatase-1 from *Entamoeba histolytica* capable of hydrolysing both 3'-phosphoadenosine 5'-phosphate and inositol 1,4-bisphosphate. *Acta Crystallogr. D Biol. Crystallogr.* 70, 2019–2031. <https://doi.org/10.1107/s1399004714010268>.
51. Rattay, S., Hufbauer, M., Hoboth, P., Sztacho, M., and Akgül, B. (2023). Viruses and phospholipids: Friends and foes during infection. *J. Med. Virol.* 95, e28658.
52. Martin, D.D., Ciulla, R.A., and Roberts, M.F. (1999). Osmoadaptation in Archaea. *Appl. Environ. Microbiol.* 65, 1815–1825. <https://doi.org/10.1128/AEM.65.5.1815-1825.1999>.
53. Heaver, S.L., Le, H.H., Tang, P., Baslé, A., Mirretta Barone, C., Vu, D.L., Waters, J.L., Marles-Wright, J., Johnson, E.L., Campopiano, D.J., et al. (2022). Characterization of inositol lipid metabolism in gut-associated Bacteroidetes. *Nat. Microbiol.* 7, 986–1000. <https://doi.org/10.1038/s41564-022-01152-6>.
54. Reynolds, T.B. (2009). Strategies for acquiring the phospholipid metabolite inositol in pathogenic bacteria, fungi and protozoa: making it and taking it. *Microbiology (Reading)* 155, 1386–1396. <https://doi.org/10.1099/mic.0.025718-0>.
55. Li, F., Hou, C.D., Lokareddy, R.K., Yang, R., Forti, F., Briani, F., and Cingolani, G. (2023). High-resolution cryo-EM structure of the *Pseudomonas* bacteriophage E217. *Nat. Commun.* 14, 4052. <https://doi.org/10.1038/s41467-023-39756-z>.
56. Garbe, J., Wesche, A., Bunk, B., Kazmierczak, M., Selezska, K., Rohde, C., Sikorski, J., Rohde, M., Jahn, D., and Schobert, M. (2010). Characterization of JG024, a *pseudomonas aeruginosa* PB1-like broad host range phage under simulated infection conditions. *BMC Microbiol.* 10, 301. <https://doi.org/10.1186/1471-2180-10-301>.
57. Wilkinson, O.J., Carrasco, C., Aicart-Ramos, C., Moreno-Herrero, F., and Dillingham, M.S. (2020). Bulk and single-molecule analysis of a bacterial

- DNA2-like helicase–nuclease reveals a single-stranded DNA looping motor. *Nucleic Acids Res.* 48, 7991–8005. <https://doi.org/10.1093/nar/gkaa562>.
58. Belotserkovskii, B.P., Tornaletti, S., D'Souza, A.D., and Hanawalt, P.C. (2018). R-loop generation during transcription: Formation, processing and cellular outcomes. *DNA Repair* 71, 69–81. <https://doi.org/10.1016/j.dnarep.2018.08.009>.
59. Hasanova, Z., Klapstova, V., Porrua, O., Steff, R., and Sebesta, M. (2023). Human senataxin is a bona fide R-loop resolving enzyme and transcription termination factor. *Nucleic Acids Res.* 51, 2818–2837. <https://doi.org/10.1093/nar/gkad092>.
60. Groh, M., Albuлесcu, L.O., Cristini, A., and Gromak, N. (2017). Senataxin: Genome Guardian at the Interface of Transcription and Neurodegeneration. *J. Mol. Biol.* 429, 3181–3195. <https://doi.org/10.1016/j.jmb.2016.10.021>.
61. Brázda, V., Havlík, J., Kolomazník, J., Trenz, O., and Štastrný, J. (2021). R-Loop Tracker: Web Access-Based Tool for R-Loop Detection and Analysis in Genomic DNA Sequences. *Int. J. Mol. Sci.* 22, 12857. <https://doi.org/10.3390/ijms222312857>.
62. Anantharaman, V., Makarova, K.S., Burroughs, A.M., Koonin, E.V., and Aravind, L. (2013). Comprehensive analysis of the HEPN superfamily: identification of novel roles in intra-genomic conflicts, defense, pathogenesis and RNA processing. *Biol. Direct* 8, 15. <https://doi.org/10.1186/1745-6150-8-15>.
63. Skružný, M., Schneider, C., Rácz, A., Weng, J., Tollervey, D., and Hurt, E. (2009). An Endoribonuclease Functionally Linked to Perinuclear mRNP Quality Control Associates with the Nuclear Pore Complexes. *PLoS Biol.* 7, e8. <https://doi.org/10.1371/journal.pbio.1000008>.
64. Wang, J., Chitsaz, F., Derbyshire, M.K., Gonzales, N.R., Gwadz, M., Lu, S., Marchler, G.H., Song, J.S., Thanki, N., Yamashita, R.A., et al. (2023). The conserved domain database in 2023. *Nucleic Acids Res.* 51, D384–D388. <https://doi.org/10.1093/nar/gkac1096>.
65. Gao, L.A., Wilkinson, M.E., Strecker, J., Makarova, K.S., Macrae, R.K., Koonin, E.V., and Zhang, F. (2022). Prokaryotic innate immunity through pattern recognition of conserved viral proteins. *Science* 377, eabm4096. <https://doi.org/10.1126/science.abm4096>.
66. Duncan, J.A., and Canna, S.W. (2018). The NLRC4 Inflammasome. *Immunol. Rev.* 287, 115–123. <https://doi.org/10.1111/immr.12607>.
67. Kibby, E.M., Conte, A.N., Burroughs, A.M., Nagy, T.A., Vargas, J.A., Whalen, L.A., Aravind, L., and Whiteley, A.T. (2023). Bacterial NLR-related proteins protect against phage. *Cell* 186, 2410–2424.e18. <https://doi.org/10.1016/j.cell.2023.04.015>.
68. Rosenstiel, P., Till, A., and Schreiber, S. (2007). NOD-like receptors and human diseases. *Microbes Infect.* 9, 648–657. <https://doi.org/10.1016/j.micinf.2007.01.015>.
69. Bauernfried, S., Scherr, M.J., Pichlmair, A., Duderstadt, K.E., and Hornung, V. (2021). Human NLRP1 is a sensor for double-stranded RNA. *Science* 371, eabd0811. <https://doi.org/10.1126/science.abd0811>.
70. Maruta, N., Burdett, H., Lim, B.Y.J., Hu, X., Desa, S., Manik, M.K., and Kobe, B. (2022). Structural basis of NLR activation and innate immune signalling in plants. *Immunogenetics* 74, 5–26. <https://doi.org/10.1007/s00251-021-01242-5>.
71. Gao, Y., Skowyra, M.L., Feng, P., and Rapoport, T.A. (2022). Protein import into peroxisomes occurs through a nuclear pore-like phase. *Science* 378, eadf3971. <https://doi.org/10.1126/science.adf3971>.
72. Baggs, E., Dagdas, G., and Krasileva, K.V. (2017). NLR diversity, helpers and integrated domains: making sense of the NLR IDentity. *Curr. Opin. Plant Biol.* 38, 59–67. <https://doi.org/10.1016/j.pbi.2017.04.012>.
73. Cebrían-Sastre, E., Martín-Blecua, I., Gullón, S., Blázquez, J., and Castañeda-García, A. (2021). Control of Genome Stability by EndoMS/NucS-Mediated Non-Canonical Mismatch Repair. *Cells* 10, 1314.
74. Takeda, K., Akimoto, C., and Kawamukai, M. (2001). Effects of the *Escherichia coli* sfsA Gene on mal Genes Expression and a DNA Binding Activity of SfsA. *Biosci. Biotechnol. Biochem.* 65, 213–217. <https://doi.org/10.1271/bbb.65.213>.
75. Ren, B., Kühn, J., Meslet-Cladiere, L., Briffotiaux, J., Norais, C., Lavigne, R., Flament, D., Ladenstein, R., and Myllykallio, H. (2009). Structure and function of a novel endonuclease acting on branched DNA substrates. *EMBO J.* 28, 2479–2489. <https://doi.org/10.1038/emboj.2009.192>.
76. Creze, C., Ligabue, A., Laurent, S., Lestini, R., Laptенок, S.P., Khun, J., Vos, M.H., Czjzek, M., Myllykallio, H., and Flament, D. (2012). Modulation of the *Pyrococcus abyssi* NucS Endonuclease Activity by Replication Clamp at Functional and Structural Levels. *J. Biol. Chem.* 287, 15648–15660. <https://doi.org/10.1074/jbc.M112.346361>.
77. Burroughs, A.M., Iyer, L.M., and Aravind, L. (2009). Natural history of the E1-like superfamily: Implications for adenylation, sulfur transfer, and ubiquitin conjugation. *Proteins* 75, 895–910. <https://doi.org/10.1002/prot.22298>.
78. Isaacson, M.K., and Ploegh, H.L. (2009). Ubiquitination, Ubiquitin-like Modifiers, and Deubiquitination in Viral Infection. *Cell Host Microbe* 5, 559–570. <https://doi.org/10.1016/j.chom.2009.05.012>.
79. Ledvina, H.E., Ye, Q., Gu, Y., Sullivan, A.E., Quan, Y., Lau, R.K., Zhou, H., Corbett, K.D., and Whiteley, A.T. (2023). An E1–E2 fusion protein primes antiviral immune signalling in bacteria. *Nature* 616, 319–325. <https://doi.org/10.1038/s41586-022-05647-4>.
80. Jenson, J.M., Li, T., Du, F., Ea, C.-K., and Chen, Z.J. (2023). Ubiquitin-like conjugation by bacterial cGAS enhances anti-phage defence. *Nature* 616, 326–331. <https://doi.org/10.1038/s41586-023-05862-7>.
81. Andryka-Cegielski, K., Soler, S., and Bartok, E. (2023). Unexpected bonds: ubiquitin-like conjugation of cGAS/CD-NTases supports their enzymatic activity and antiphage defense. *Signal Transduct. Target. Ther.* 8, 308. <https://doi.org/10.1038/s41392-023-01549-7>.
82. Yan, Y., Xiao, J., Yan, Y., Xiao, J., Huang, F., Yu, B., Cheng, R., Wu, H., Lu, X., Wang, X., Oyejobi, G.K., Robinson, C.V., et al. (2023). Ubiquitin-like cGAS chain formation by a super enzyme activates anti-phage response. *Nat. Microbiol.* 9, 1566–1578. <https://doi.org/10.1101/2022.05.25.493364>.
83. Pettinati, I., Brem, J., Lee, S.Y., McHugh, P.J., and Schofield, C.J. (2016). The Chemical Biology of Human Metallo-β-Lactamase Fold Proteins. *Trends Biochem. Sci.* 41, 338–355. <https://doi.org/10.1016/j.tibs.2015.12.007>.
84. van Kempen, M., Kim, S.S., Tumescheit, C., Mirdita, M., Lee, J., Gilchrist, C.L.M., Söding, J., and Steinegger, M. (2024). Fast and accurate protein structure search with Foldseek. *Nat. Biotechnol.* 42, 243–246. <https://doi.org/10.1038/s41587-023-01773-0>.
85. Baker, J.A., Simkovic, F., Taylor, H.M.C., and Rigden, D.J. (2016). Potential DNA binding and nuclease functions of ComEC domains characterized in silico. *Proteins* 84, 1431–1442. <https://doi.org/10.1002/prot.25088>.
86. O'Neill, L.A.J., and Bowie, A.G. (2007). The family of five: TIR-domain-containing adaptors in Toll-like receptor signalling. *Nat. Rev. Immunol.* 7, 353–364. <https://doi.org/10.1038/nri2079>.
87. Luo, L., Lucas, R.M., Liu, L., and Stow, J.L. (2019). Signalling, sorting and scaffolding adaptors for Toll-like receptors. *J. Cell Sci.* 133, jcs239194. <https://doi.org/10.1242/jcs.239194>.
88. Ademi, M., Yang, X., Coleman, M.P., and Gilley, J. (2022). Natural variants of human SARM1 cause both intrinsic and dominant loss-of-function influencing axon survival. *Sci. Rep.* 12, 13846. <https://doi.org/10.1038/s41598-022-18052-8>.
89. Janssens, S., and Beyaert, R. (2003). Role of Toll-Like Receptors in Pathogen Recognition. *Clin. Microbiol. Rev.* 16, 637–646. <https://doi.org/10.1128/cmr.16.4.637-646.2003>.
90. Sabonis, D., Avraham, C., Lu, A., Herbst, E., Silanskas, A., Leavitt, A., Yirmiya, E., Zaremba, M., Amitai, G., Kranzusch, P.J., et al. (2024). TIR domains produce histidine-ADPR conjugates as immune signaling molecules in bacteria. Preprint at bioRxiv. <https://doi.org/10.1101/2024.01.03.573942>.

91. Tal, N., Morehouse, B.R., Millman, A., Stokar-Avihail, A., Avraham, C., Fedorenko, T., Yirmiya, E., Herbst, E., Brandis, A., Mehlman, T., et al. (2021). Cyclic CMP and cyclic UMP mediate bacterial immunity against phages. *Cell* *184*, 5728–5739.e16. <https://doi.org/10.1016/j.cell.2021.09.031>.
92. Rousset, F., and Sorek, R. (2023). The evolutionary success of regulated cell death in bacterial immunity. *Curr. Opin. Microbiol.* *74*, 102312. <https://doi.org/10.1016/j.mib.2023.102312>.
93. Duncan-Lowey, B., Tal, N., Johnson, A.G., Rawson, S., Mayer, M.L., Doron, S., Millman, A., Melamed, S., Fedorenko, T., Kacen, A., et al. (2023). Cryo-EM structure of the RADAR supramolecular anti-phage defense complex. *Cell* *186*, 987–998.e15. <https://doi.org/10.1016/j.cell.2023.01.012>.
94. Gao, Y., Luo, X., Li, P., Li, Z., Ye, F., Liu, S., and Gao, P. (2023). Molecular basis of RADAR anti-phage supramolecular assemblies. *Cell* *186*, 999–1012.e20. <https://doi.org/10.1016/j.cell.2023.01.026>.
95. Ofir, G., Melamed, S., Sberro, H., Mukamel, Z., Silverman, S., Yaakov, G., Doron, S., and Sorek, R. (2018). DISARM is a widespread bacterial defense system with broad anti-phage activities. *Nat. Microbiol.* *3*, 90–98. <https://doi.org/10.1038/s41564-017-0051-0>.
96. Cheng, R., Huang, F., Lu, X., Yan, Y., Yu, B., Wang, X., and Zhu, B. (2023). Prokaryotic Gabija complex senses and executes nucleotide depletion and DNA cleavage for antiviral defense. *Cell Host Microbe* *31*, 1331–1344.e5. <https://doi.org/10.1016/j.chom.2023.06.014>.
97. Ran, F.A., Hsu, P.D., Wright, J., Agarwala, V., Scott, D.A., and Zhang, F. (2013). Genome engineering using the CRISPR-Cas9 system. *Nat. Protoc.* *8*, 2281–2308. <https://doi.org/10.1038/nprot.2013.143>.
98. Huang, C.-H., Lee, K.-C., and Doudna, J.A. (2018). Applications of CRISPR-Cas Enzymes in Cancer Therapeutics and Detection. *Trends Cancer* *4*, 499–512. <https://doi.org/10.1016/j.trecan.2018.05.006>.
99. Guo, B., Yang, L., Wang, Y., Zhao, C., Zhang, X., Tang, Y., Wang, Y., Shen, H., Gao, S., and Wang, P. (2023). *Pyrococcus furiosus* Argonaute with isothermal amplification for fast and ultra-sensitive diagnosis of acute hepatopancreatic necrosis disease in shrimp. *Aquaculture* *575*, 739821. <https://doi.org/10.1016/j.aquaculture.2023.739821>.
100. Roberts, R.J. (2005). How restriction enzymes became the workhorses of molecular biology. *Proc. Natl. Acad. Sci. USA* *102*, 5905–5908. <https://doi.org/10.1073/pnas.0500923102>.
101. Fu, L., Xie, C., Jin, Z., Tu, Z., Han, L., Jin, M., Xiang, Y., and Zhang, A. (2019). The prokaryotic Argonaute proteins enhance homology sequence-directed recombination in bacteria. *Nucleic Acids Res.* *47*, 3568–3579. <https://doi.org/10.1093/nar/gkz040>.
102. Jackson, D.A., Symons, R.H., and Berg, P. (1972). Biochemical Method for Inserting New Genetic Information into DNA of Simian Virus 40: Circular SV40 DNA Molecules Containing Lambda Phage Genes And The Galactose Operon of Escherichia coli. *Proc. Natl. Acad. Sci. USA* *69*, 2904–2909. <https://doi.org/10.1073/pnas.69.10.2904>.
103. van Beijouw, S.P.B., Sanders, J., Rodríguez-Molina, A., and Brouns, S.J.J. (2023). RNA-targeting CRISPR-Cas systems. *Nat. Rev. Microbiol.* *21*, 21–34. <https://doi.org/10.1038/s41579-022-00793-y>.
104. Jumper, J., Evans, R., Pritzel, A., Green, T., Figurnov, M., Ronneberger, O., Tunyasuvunakool, K., Bates, R., Židek, A., Potapenko, A., et al. (2021). Highly accurate protein structure prediction with AlphaFold. *Nature* *596*, 583–589. <https://doi.org/10.1038/s41586-021-03819-2>.
105. Mirdita, M., Schütze, K., Moriwaki, Y., Heo, L., Ovchinnikov, S., and Steinegger, M. (2022). ColabFold: making protein folding accessible to all. *Nat. Methods* *19*, 679–682. <https://doi.org/10.1038/s41592-022-01488-1>.
106. Morris, G.M., Huey, R., Lindstrom, W., Sanner, M.F., Belew, R.K., Goodsell, D.S., and Olson, A.J. (2009). AutoDock4 and AutoDockTools4: Automated docking with selective receptor flexibility. *J. Comput. Chem* *30*, 2785–2791. <https://doi.org/10.1002/jcc.21256>.
107. Trott, O., and Olson, A.J. (2010). AutoDock Vina: Improving the speed and accuracy of docking with a new scoring function, efficient optimization, and multithreading. *J. Comput. Chem.* *31*, 455–461. <https://doi.org/10.1002/jcc.21334>.
108. Quinlan, A.R., and Hall, I.M. (2010). BEDTools: a flexible suite of utilities for comparing genomic features. *Bioinformatics* *26*, 841–842. <https://doi.org/10.1093/bioinformatics/btq033>.
109. Altschul, S.F., Gish, W., Miller, W., Myers, E.W., and Lipman, D.J. (1990). Basic local alignment search tool. *J. Mol. Biol.* *215*, 403–410. [https://doi.org/10.1016/S0022-2836\(05\)80360-2](https://doi.org/10.1016/S0022-2836(05)80360-2).
110. Li, H., and Durbin, R. (2009). Fast and accurate short read alignment with Burrows–Wheeler transform. *Bioinformatics* *25*, 1754–1760. <https://doi.org/10.1093/bioinformatics/btp324>.
111. Gilchrist, C.L.M., Booth, T.J., van Wersch, B., van Grieken, L., Medema, M.H., and Chooi, Y.-H. (2021). cblastercblaster: a remote search tool for rapid identification and visualization of homologous gene clusters. *Bioinform. Adv.* *1*, vbab016. <https://doi.org/10.1093/bioadv/vbab016>.
112. Thompson, J.D., Higgins, D.G., and Gibson, T.J. (1994). CLUSTAL W: improving the sensitivity of progressive multiple sequence alignment through sequence weighting, position-specific gap penalties and weight matrix choice. *Nucleic Acids Res.* *22*, 4673–4680. <https://doi.org/10.1093/nar/22.22.4673>.
113. Larkin, M.A., Blackshields, G., Brown, N.P., Chenna, R., McGettigan, P.A., McWilliam, H., Valentin, F., Wallace, I.M., Wilm, A., Lopez, R., et al. (2007). Clustal W and Clustal X version 2.0. *Bioinformatics* *23*, 2947–2948. <https://doi.org/10.1093/bioinformatics/btm404>.
114. García, J.C., Guadagno, A., Paytuví-Gallart, A., Saera-Vila, A., Gianmaria Amoroso, C., D’Esposito, D., Andolfo, G., Cigliano, R.A., Sanseverino, W., and Ercolano, M.R. (2022). PRGdb 4.0: an updated database dedicated to genes involved in plant disease resistance process. *Nucleic Acids Res* *50*, D1483–D1490. <https://doi.org/10.1093/nar/gkbb1087>.
115. Robinson, M.D., McCarthy, D.J., and Smyth, G.K. (2010). edgeR: a Bioconductor package for differential expression analysis of digital gene expression data. *Bioinformatics* *26*, 139–140. <https://doi.org/10.1093/bioinformatics/btp616>.
116. Blighe, K., Rana, S., and Lewis, M. (2023). EnhancedVolcano: Publication-ready volcano plots with enhanced colouring and labeling. *Bioconductor*. <https://bioconductor.org/packages/EnhancedVolcano>.
117. Price, M.N., Dehal, P.S., and Arkin, A.P. (2010). FastTree 2 – Approximately Maximum-Likelihood Trees for Large Alignments. *PLoS One* *5*, e9490. <https://doi.org/10.1371/journal.pone.0009490>.
118. Biegert, A., and Söding, J. (2008). De novo identification of highly diverged protein repeats by probabilistic consistency. *Bioinformatics* *24*, 807–814. <https://doi.org/10.1093/bioinformatics/btn039>.
119. Finn, R.D., Clements, J., and Eddy, S.R. (2011). HMMER web server: interactive sequence similarity searching. *Nucleic Acids Res.* *39*, W29–W37. <https://doi.org/10.1093/nar/gkr367>.
120. Thorvaldsdóttir, H., Robinson, J.T., and Mesirov, J.P. (2013). Integrative Genomics Viewer (IGV): high-performance genomics data visualization and exploration. *Brief. Bioinform.* *14*, 178–192. <https://doi.org/10.1093/bib/bbs017>.
121. Minh, B.Q., Schmidt, H.A., Chernomor, O., Schrempf, D., Woodhams, M.D., von Haeseler, A., and Lanfear, R. (2020). IQ-TREE 2: New Models and Efficient Methods for Phylogenetic Inference in the Genomic Era. *Mol. Biol. Evol.* *37*, 1530–1534. <https://doi.org/10.1093/molbev/msaa015>.
122. Letunic, I., and Bork, P. (2019). Interactive Tree Of Life (iTOL) v4: recent updates and new developments. *Nucleic Acids Res.* *47*, W256–W259. <https://doi.org/10.1093/nar/gkz239>.
123. Li, H. (2018). Minimap2: pairwise alignment for nucleotide sequences. *Bioinformatics* *34*, 3094–3100. <https://doi.org/10.1093/bioinformatics/bty191>.
124. Edgar, R.C. (2022). Muscle5: High-accuracy alignment ensembles enable unbiased assessments of sequence homology and phylogeny. *Nat. Commun.* *13*, 6968. <https://doi.org/10.1038/s41467-022-34630-w>.

125. Dai, C., Qu, Y., Wu, W., Li, S., Chen, Z., Lian, S., and Jing, J. (2023). QSP: An open sequence database for quorum sensing related gene analysis with an automatic annotation pipeline. *Water Res.* 235, 119814. <https://doi.org/10.1016/j.watres.2023.119814>.
126. O'Boyle, N.M., Banck, M., James, C.A., Morley, C., Vandermeersch, T., and Hutchison, G.R. (2011). Open Babel: An open chemical toolbox. *J. Cheminform.* 3, 33. <https://doi.org/10.1186/1758-2946-3-33>.
127. Payne, L.J., Todeschini, T.C., Wu, Y., Perry, B.J., Ronson, C.W., Fineran, P.C., Nobrega, F.L., and Jackson, S.A. (2021). Identification and classification of antiviral defence systems in bacteria and archaea with PADLOC reveals new system types. *Nucleic Acids Res.* 49, 10868–10878. <https://doi.org/10.1093/nar/gkab883>.
128. Treangen, T.J., Ondov, B.D., Koren, S., and Phillippy, A.M. (2014). The Harvest suite for rapid core-genome alignment and visualization of thousands of intraspecific microbial genomes. *Genome Biol.* 15, 524. <https://doi.org/10.1186/s13059-014-0524-x>.
129. Käll, L., Krogh, A., and Sonnhammer, E.L.L. (2004). A Combined Transmembrane Topology and Signal Peptide Prediction Method. *J. Mol. Biol.* 338, 1027–1036. <https://doi.org/10.1016/j.jmb.2004.03.016>.
130. Gautreau, G., Bazin, A., Gachet, M., Planel, R., Burlot, L., Dubois, M., Perrin, A., Médigue, C., Calteau, A., Cruveiller, S., et al. (2020). PPanGGOLiN: Depicting microbial diversity via a partitioned pangenome graph. *PLoS Comput. Biol.* 16, e1007732. <https://doi.org/10.1371/journal.pcbi.1007732>.
131. Altschul, S.F., Madden, T.L., Schäffer, A.A., Zhang, J., Zhang, Z., Miller, W., and Lipman, D.J. (1997). Gapped BLAST and PSI-BLAST: a new generation of protein database search programs. *Nucleic Acids Res.* 25, 3389–3402. <https://doi.org/10.1093/nar/25.17.3389>.
132. Delano, W.L. (2002). PyMOL: An Open-Source Molecular Graphics Tool. http://www.ccp4.ac.uk/newsletters/newsletter40/11_pymol.pdf.
133. Jenjaroenpun, P., Wongsurawat, T., Yenamandra, S.P., and Kuznetsov, V.A. (2015). QmRLFS-finder: a model, web server and stand-alone tool for prediction and analysis of R-loop forming sequences. *Nucleic Acids Res.* 43, W527–W534. <https://doi.org/10.1093/nar/gkv344>.
134. Li, H., Handsaker, B., Wysoker, A., Fennell, T., Ruan, J., Homer, N., Marth, G., Abecasis, G., and Durbin, R.; 1000 Genome Project Data Processing Subgroup (2009). The Sequence Alignment/Map format and SAMtools. *Bioinformatics* 25, 2078–2079. <https://doi.org/10.1093/bioinformatics/btp352>.
135. Shen, W., Le, S., Li, Y., and Hu, F. (2016). SeqKit: A Cross-Platform and Ultrafast Toolkit for FASTA/Q File Manipulation. *PLoS One* 11, e0163962. <https://doi.org/10.1371/journal.pone.0163962>.
136. Almagro Armenteros, J.J., Tsirigos, K.D., Sønderby, C.K., Petersen, T.N., Winther, O., Brunak, S., von Heijne, G., and Nielsen, H. (2019). SignalP 5.0 improves signal peptide predictions using deep neural networks. *Nat. Biotechnol.* 37, 420–423. <https://doi.org/10.1038/s41587-019-0036-z>.
137. MacLean, B., Tomazela, D.M., Shulman, N., Chambers, M., Finney, G.L., Frewen, B., Kern, R., Tabb, D.L., Liebler, D.C., and MacCoss, M.J. (2010). Skyline: an open source document editor for creating and analyzing targeted proteomics experiments. *Bioinformatics* 26, 966–968. <https://doi.org/10.1093/bioinformatics/btq054>.
138. Capella-Gutiérrez, S., Silla-Martínez, J.M., and Gabaldón, T. (2009). trimAl: a tool for automated alignment trimming in large-scale phylogenetic analyses. *Bioinformatics* 25, 1972–1973. <https://doi.org/10.1093/bioinformatics/btp348>.
139. Saha, C.K., Sanches Pires, R., Brolin, H., Delannoy, M., and Atkinson, G.C. (2021). FlaGs and webFlaGs: discovering novel biology through the analysis of gene neighbourhood conservation. *Bioinformatics* 37, 1312–1314. <https://doi.org/10.1093/bioinformatics/btaa788>.
140. Rousset, F., Yirmiya, E., Neshet, S., Brandis, A., Mehlman, T., Itkin, M., Malitsky, S., Millman, A., Melamed, S., and Sorek, R. (2023). A conserved family of immune effectors cleaves cellular ATP upon viral infection. *Cell* 186, 3619–3631.e13. <https://doi.org/10.1016/j.cell.2023.07.020>.
141. Bazin, A., Gautreau, G., Médigue, C., Vallenet, D., and Calteau, A. (2020). panRGP: a pangenome-based method to predict genomic islands and explore their diversity. *Bioinformatics* 36, i651–i658. <https://doi.org/10.1093/bioinformatics/btaa792>.
142. Mistry, J., Finn, R.D., Eddy, S.R., Bateman, A., and Punta, M. (2013). Challenges in homology search: HMMER3 and convergent evolution of coiled-coil regions. *Nucleic Acids Res.* 41, e121. <https://doi.org/10.1093/nar/gkt263>.
143. Choi, K.-H., Kumar, A., and Schweizer, H.P. (2006). A 10-min method for preparation of highly electrocompetent *Pseudomonas aeruginosa* cells: Application for DNA fragment transfer between chromosomes and plasmid transformation. *J. Microbiol. Methods* 64, 391–397. <https://doi.org/10.1016/j.mimet.2005.06.001>.
144. Mazzocco, A., Waddell, T.E., Lingohr, E., and Johnson, R.P. (2009). Enumeration of Bacteriophages Using the Small Drop Plaque Assay System. In *Bacteriophages: Methods and Protocols*, Volume 1: Isolation, Characterization, and Interactions, M.R.J. Clokie and A.M. Kropinski, eds. (Humana Press), pp. 81–85. https://doi.org/10.1007/978-1-60327-164-6_9.
145. Stokar-Avihail, A., Fedorenko, T., Hör, J., Garb, J., Leavitt, A., Millman, A., Shulman, G., Wojtania, N., Melamed, S., Amitai, G., et al. (2023). Discovery of phage determinants that confer sensitivity to bacterial immune systems. *Cell* 186, 1863–1876.e16. <https://doi.org/10.1016/j.cell.2023.02.029>.
146. Frirdich, E., Bouwman, C., Vinogradov, E., and Whitfield, C. (2005). The Role of Galacturonic Acid in Outer Membrane Stability in *Klebsiella pneumoniae*. *J. Biol. Chem.* 280, 27604–27612. <https://doi.org/10.1074/jbc.M504987200>.
147. Kulikov, E.E., Golomidova, A.K., Prokhorov, N.S., Ivanov, P.A., and Letarov, A.V. (2019). High-throughput LPS profiling as a tool for revealing of bacteriophage infection strategies. *Sci. Rep.* 9, 2958. <https://doi.org/10.1038/s41598-019-39590-8>.
148. Feltwell, T., Dorman, M.J., Goulding, D.A., Parkhill, J., and Short, F.L. (2019). Separating Bacteria by Capsule Amount Using a Discontinuous Density Gradient. *J. Vis. Exp.* 143, e58679. <https://doi.org/10.3791/58679>.
149. Tipton, K.A., and Rather, P.N. (2019). Extraction and Visualization of Capsular Polysaccharide from *Acinetobacter baumannii*. In *Acinetobacter baumannii: Methods and Protocols*, I. Biswas and P.N. Rather, eds. (Springer), pp. 227–231. https://doi.org/10.1007/978-1-4939-9118-1_21.
150. Jenjaroenpun, P., Wongsurawat, T., Yenamandra, S.P., and Kuznetsov, V.A. (2015). QmRLFS-finder: a model, web server and stand-alone tool for prediction and analysis of R-loop forming sequences. *Nucleic Acids Res.* 43, W527–W534. <https://doi.org/10.1093/nar/gkv344>.
151. UniProt Consortium (2014). UniProt: a hub for protein information. *Nucleic Acids Res.* 43, D204–D212. <https://doi.org/10.1093/nar/gku989>.
152. Hunter, S., Apweiler, R., Attwood, T.K., Bairoch, A., Bateman, A., Binns, D., Bork, P., Das, U., Daugherty, L., Duquenne, L., et al. (2009). InterPro: the integrative protein signature database. *Nucleic Acids Res.* 37, D211–D215. <https://doi.org/10.1093/nar/gkn785>.
153. Letunic, I., and Bork, P. (2021). Interactive Tree Of Life (iTOL) v5: an online tool for phylogenetic tree display and annotation. *Nucleic Acids Res.* 49, W293–W296. <https://doi.org/10.1093/nar/gkab301>.

STAR★METHODS

KEY RESOURCES TABLE

| REAGENT or RESOURCE | SOURCE | IDENTIFIER |
|--|---------------------|----------------|
| Bacterial and virus strains | | |
| N1520 | UMC Utrecht | N/A |
| K6156 | UMC Utrecht | N/A |
| L1165 | UMC Utrecht | N/A |
| L0213 | UMC Utrecht | N/A |
| L0665 | UMC Utrecht | N/A |
| L1264 | UMC Utrecht | N/A |
| PAO1 | Fagenbank | N/A |
| vB_PaeP_FBPa3 | Fagenbank | N/A |
| vB_PaeM_FBPa10 | Fagenbank | N/A |
| vB_PaeP_FBPa18 | Fagenbank | N/A |
| vB_PaeS_FBPa28 | Fagenbank | N/A |
| vB_PaeM_FBPa34 | Fagenbank | N/A |
| vB_PaeM_FBPa36 | Fagenbank | N/A |
| vB_PaeS_FBPa53 | Fagenbank | N/A |
| PP7 | LGC Standards | ATCC-15692-B4 |
| Chemicals, peptides, and recombinant proteins | | |
| 2-mercaptoethanol | Merck | Cat# M3148 |
| Acetonitrile | Biosolve | Cat# 1200702 |
| Agar | Sigma-Aldrich | Cat# 05039 |
| Agarose | Promega Corporation | Cat# V3125 |
| Ammonium acetate | Sigma-Aldrich | Cat# 238074 |
| Ammonium formate | Supelco | Cat# 70221 |
| Ampicillin | Carl Roth | Cat# K029.4 |
| BamHI-HF | New England Biolabs | Cat# R3136S |
| B-PER Bacterial Protein Extraction Reagent | Fisher Scientific | Cat# 78243 |
| Bio-Safe™ Coomassie Stain | Bio-Rad | Cat# 1610786 |
| Calcium chloride | Acros | Cat# 10577372 |
| Carbenicillin | Fisher Scientific | Cat# BP2648-5 |
| D-myo-Inositol 1-monophosphate dipotassium salt | Sigma-Aldrich | Cat# 59937-1MG |
| DNase | Sigma-Aldrich | Cat# DN25 |
| DpnI | New England Biolabs | Cat# R0176S |
| EcoRI-HF | New England Biolabs | Cat# R3101S |
| FastAP | Fisher Scientific | Cat# EF0651 |
| Glycerol | ACROS Organics | Cat# 10296200 |
| Lithium chloride | Merck Sigma | Cat# 10577372 |
| Lysozyme Broth (LB) | Sigma-Aldrich | Cat# L3022 |
| Lysozyme | Sigma-Aldrich | Cat# 837059001 |
| Magnesium chloride hexahydrate | Sigma-Aldrich | Cat# 7791-18-6 |
| Myo-inositol | Sigma-Aldrich | Cat# 57570-25G |
| MOPS buffer | GenScript | Cat# M00138 |
| NEB 5-alpha competent E. coli | New England Biolabs | Cat# C2987H |
| RNase A, DNase and protease-free (10 mg/mL) | Thermo Fisher | Cat# EN0531 |

(Continued on next page)

Continued

| REAGENT or RESOURCE | SOURCE | IDENTIFIER |
|--|---------------------|------------------|
| Percoll | Sigma-Aldrich | Cat# P1644-100ML |
| Phosphate buffered saline | Calbiochem | Cat# 524650-EA |
| Proteinase K | Sigma-Aldrich | Cat# P2308-25MG |
| Q5 DNA polymerase | New England Biolabs | Cat# M0491L |
| Sarkosyl | Sigma-Aldrich | Cat# L9150-50G |
| Sodium chloride | Fisher Scientific | Cat# AC424290010 |
| Sodium dodecyl sulfate | Sigma-Aldrich | Cat# 8.17034 |
| SurePAGE™, Bis-Tris, 10x8, 4-12%, 12 wells | GenScript | Cat# M00653 |
| T4 DNA Ligase | New England Biolabs | Cat# M0202S |
| TAE 40X | Promega Corporation | Cat# V4281 |

Critical commercial assays

| | | |
|---|--------------------------|-------------|
| DNA Clean & Concentrator Kit | Zymo Research | Cat# D4029 |
| GeneJET Plasmid Miniprep Kit | Thermo Fisher Scientific | Cat# K0503 |
| GeneJET Genomic DNA Purification Kit | Thermo Fisher Scientific | Cat# K0721 |
| NAD/NADH Quantification Kit | Sigma-Aldrich | Cat# MAK037 |
| NEBuilder® HiFi DNA Assembly Master Mix | New England Biolabs | Cat# E2621L |
| Pierce BCA Protein Assay Kit | Thermo Fisher Scientific | Cat# 23225 |
| Qubit RNA High Sensitivity (HS) Assay Kit | Thermo Fisher Scientific | Cat# Q32852 |
| RNase-Free DNase Set | Qiagen | Cat# 79254 |
| RNeasy Mini Kit (50) | Qiagen | Cat# 74104 |
| SilverQuest™ Silver Staining Kit | Thermo Fisher Scientific | Cat# LC6070 |
| Zymoclean Gel DNA Recovery Kit | Zymo Research | Cat# D4002 |

Deposited data

| | | |
|--|------------|---|
| Raw data for bioinformatic and experimental analysis. | This study | https://doi.org/10.5281/zenodo.10210781 |
| Raw data for RNA-seq and DNA nanopore sequencing experiments | This study | https://www.ncbi.nlm.nih.gov/bioproject/1112814 |

Oligonucleotides

| | | |
|---|-----|-----|
| All the DNA oligonucleotides are listed in Table S6 | IDT | N/A |
|---|-----|-----|

Recombinant DNA

| | | |
|---|-----|-----|
| All plasmids are listed and described in Table S7 | N/A | N/A |
|---|-----|-----|

Software and algorithms

| | | |
|----------------------------|---|---|
| Adobe Illustrator 26.0.1 | Adobe | N/A |
| Adobe Photoshop CC 2018 | Adobe | N/A |
| AlphaFold v2.3.2 | Jumper et al. ¹⁰⁴ Mirdita et al. ¹⁰⁵ | https://github.com/deepmind/alphafold/releases |
| AutoDockTools v4.2.6 | Morris et al. 2009 ¹⁰⁶ | https://ccsb.scripps.edu/mgltools/ |
| Autodock vina | Trott and Olson 2010 ¹⁰⁷ | https://vina.scripps.edu/ |
| Bedtools intersect v2.31.1 | Quinlan et al. ¹⁰⁸ | https://github.com/arq5x/bedtools2/releases |
| Blastp | Altschul et al. ¹⁰⁹ | https://blast.ncbi.nlm.nih.gov/Blast.cgi?PAGE=Proteins |
| Bwa v0.7.18 | Li and Durbin ¹¹⁰ | https://github.com/lh3/bwa |
| cblaster v1.3.18 | Gilchrist et al. ¹¹¹ | https://github.com/gamcil/cblaster |
| ChimeraX | University of California, San Francisco (UCSF) | N/A |
| Clustal W v2.1 | Thompson et al. ¹¹² , Larkin et al. 2007 ¹¹³ | http://www.clustal.org/clustal2/ |
| Dali | Holm and Laakso ⁴⁴ | http://ekhidna2.biocenter.helsinki.fi/dali/ |

(Continued on next page)

Continued

| REAGENT or RESOURCE | SOURCE | IDENTIFIER |
|-----------------------------------|--|---|
| DRAGO3 | Garcia et al., 2021 ¹¹⁴ | http://prgdb.org/prgdb4/drago3 |
| DefenseFinder v1.0.9 | Tesson et al. ²⁰ | https://github.com/mdmparis/defense-finder |
| EdgeR v4.0.2 | Robinson et al. ¹¹⁵ | https://bioconductor.org/packages/release/bioc/html/edgeR.html |
| EnhancedVolcano R package v1.20.0 | Blighe et al. ¹¹⁶ | https://bioconductor.org/packages/release/bioc/html/EnhancedVolcano.html |
| Eukprot v3 | Richter et al. ³⁵ | https://evocellbio.com/eukprot/ |
| FastTree v2.1.11 | Price et al. ¹¹⁷ | http://www.microbesonline.org/fasttree/ |
| Filterlong v0.2.1 | N/A | https://github.com/rwick/Filterlong |
| Foldseek v6 | van Kempen et al. ⁸⁴ | https://github.com/steineggerlab/foldseek |
| GraphPad Prism 7.00 | GraphPad | N/A |
| HHrepID | Biegert and Söding ¹¹⁸ | https://toolkit.tuebingen.mpg.de/tools/hhrepid |
| Hmmbuild v3.3.2 | Finn et al. ¹¹⁹ | https://anaconda.org/bioconda/hmmer |
| HMMer v3.3.2 | Finn et al. ¹¹⁹ | https://github.com/EddyRivasLab/hmmer |
| Hmmsearch | Finn et al. ¹¹⁹ | https://github.com/madscientist01/hmmsearch |
| Integrative Genomics Viewer (IGV) | Thorvaldsdóttir et al. ¹²⁰ | https://igv.org/doc/desktop/ |
| iQ-Tree2 v2.2.6 | Minh et al. ¹²¹ | https://github.com/iqtree/iqtree2/ |
| iTol v1.0 | Letunic and Bork ¹²² | https://itol.embl.de/ |
| MassHunter v10.1 | Agilent | https://www.agilent.com/en/product/software-informatics/mass-spectrometry-software/data-analysis/quantitative-analysis |
| Minimap2 v2.28 | Li ¹²³ | https://github.com/lh3/minimap2/releases |
| Muscle v5.3 | Edgar ¹²⁴ | https://www.drive5.com/muscle/ |
| Mmseqs2 v15.6 | Dai et al. ¹²⁵ | https://github.com/soedinglab/MMseqs2 |
| OpenBabel v2.4.0 | O'Boyle et al. 2011 ¹²⁶ | https://openbabel.org/wiki/Main_Page |
| PADLOC v1.1.0 | Payne et al. ¹²⁷ | https://github.com/padlocbio/padloc |
| Parsnp v1.7.4 | Treangen et al. ¹²⁸ | https://github.com/marbl/harvest |
| Phobius v1.01 | Käll et al. ¹²⁹ | https://bioweb.pasteur.fr/packages/pack@phobius@1.01 |
| PPanGGOLiN v1.2.74 | Gautreau et al. ¹³⁰ | https://github.com/labgem/PPanGGOLiN |
| PRGdb v4.0 | Garcia et al., 2021 | http://prgdb.org/prgdb4/ |
| PSI-BLAST | Altschul et al. ¹³¹ | https://blast.ncbi.nlm.nih.gov/Blast.cgi?PAGE_TYPE=BlastSearch&PROGRAM=blastp&BLAST_PROGRAMS=psiBlast |
| PyMol v2.5.4 | Delano, 2002 ¹³² | https://pymol.org/2/ |
| QmRLFS-finder | Jenjaroenpun et al., 2024 ¹³³ | http://r-loop.org/?pg=qmrlfs-finder |
| R-loop tracker | Brázda et al. ⁶¹ | https://bioinformatics.ibp.cz/#/analyse/rloopr |
| Samtools v1.20 | Li et al. ¹³⁴ | https://github.com/samtools/samtools/releases/ |
| Seqkit v2.7.0 (rmdup) | Shen et al. ¹³⁵ | https://github.com/shenwei356/seqkit/releases |
| SignalP v5.0 | Almagro Armenteros et al. ¹³⁶ | https://services.healthtech.dtu.dk/services/SignalP-5.0/ |
| Skyline | MacLean et al. ¹³⁷ | https://skyline.ms/project/home/software/Skyline/begin.view |
| trimAl v1.8 | Capella-Gutiérrez et al. ¹³⁸ | https://vicfero.github.io/trimal/ |
| Webflags v1 | Saha et al. ¹³⁹ | https://github.com/GCA-VH-lab/FlaGs2 |

Other

| | | |
|--|--------------------|--------------------------|
| Agilent G6460C Triple Quad Mass Spectrometer | Agilent | Cat# G6460C |
| Bio-Rad Gel Doc XR+ | Bio-Rad | Cat# Bio-Rad Gel Doc XR+ |
| Epoch 2 microplate reader | Biotek Instruments | Cat# EPOCH2 |
| Nanophotometer | Implen | Cat# NP80 |

(Continued on next page)

Continued

| REAGENT or RESOURCE | SOURCE | IDENTIFIER |
|--|--------------------------|----------------|
| Qubit 4 Fluorometer | Thermo Fisher Scientific | Cat# Q33238 |
| ACQUITY Premier Peptide CSH C18 Column, 130 Å, 1.7 μm, 2.1 x 50 mm with Premier VanGuard FIT Guard | Waters Corporation | Cat# 186010709 |

RESOURCE AVAILABILITY

Lead contact

Further information and requests for resources and reagents should be directed to and will be fulfilled by the lead contact, Stan J. J. Brouns (stanbrouns@gmail.com).

Materials availability

All unique bacterial strains, phages, and plasmids generated in this study are available from the [lead contact](#) without restriction.

Data and code availability

- Raw data are publicly available as of the date of publication. Accession numbers are listed in the [key resources table](#).
- This paper does not report original code.
- Any additional information required to reanalyze the data reported in this paper is available from the [lead contact](#) upon request.

EXPERIMENTAL MODEL AND SUBJECT DETAILS

Bacteria and phages

A set of 6 clinical isolates of *P. aeruginosa* obtained from the University Medical Centre Utrecht (UMCU)¹⁰ was used to amplify putative eukaryotic-like defense systems. *Escherichia coli* strain Dh5α and *P. aeruginosa* strain PAO1 were used for cloning of plasmid pUCP20 with the defense systems. All bacterial strains were grown in Lysogeny Broth (LB) at 37 °C and 180 rpm, or in LB agar (LBA, 1.5 % agar (w/v)) plates at 37 °C. Strains containing plasmid pUCP20 were grown in media supplemented with 100 μg/ml of ampicillin (for *E. coli*) or 200 μg/ml of carbenicillin (for *P. aeruginosa*). All phages used in this study were obtained from the Fagenbank,¹⁰ except for *Pseudomonas* phage PP7 which was acquired from LGC Standards. Phages were amplified in liquid media with PAO1, centrifuged at 3,000 × *g* for 15 min, filter-sterilized (0.2 μm PES), and stored as phage lysates at 4 °C until further use.

METHOD DETAILS

Identification of anti-phage defense systems

We searched for defense systems using PADLOC v1.1.0 with PADLOC-DB v1.4.0,¹²⁷ and DefenseFinder v1.0.9 with defense-finder-models v1.2.2,²⁰ and the HMMs with completeness rules and thresholds as applied in Gao et al.⁶ Additionally, Detocs was searched for using blastp¹⁰⁹ (> 0.7 subject length / query length < 1.5; 0.7 > query coverage < 1.3; evalue < 1e-9) and found complete if all three genes were present with a maximum of 1 gene in between.¹⁴⁰ We observed *dtcB* to fail gene annotation, thus we manually checked for its presence when *dtcA* and *dtcC* were identified within close proximity (1 gene in between).

Identification of conserved gene clusters within the variable regions of *Pseudomonas aeruginosa*

We used PPanGGOLiN v1.2.74^{130,141} to identify the conserved gene clusters within the variable regions of all 541 complete *P. aeruginosa* assemblies from the Refseq database on June 16, 2022. Functional domains were identified using HMMER v3.3.2¹⁴² in combination with the Pfam-A models v36.0.

We utilized Eukprot v3³⁵ to find homologs of innate immune proteins from vertebrates and plants. For the vertebrate innate proteins, we built HMM profiles of the aligned InnateDB³³ in June 2022 using MUSCLE v5.1¹²⁴ and hmmbuild.¹¹⁹ We applied the same method to find homologs of plant innate proteins, using the Plant Resistance Genes database (PRGd) v4.0.³⁴ Additionally, we applied DRAGO3³⁴ to search for plant pathogen recognition proteins. For both vertebrate and plant innate proteins, we created a custom database of functional domains found to be associated with innate defense in literature (Table S1). This list of functional domains and the created HMM profiles were then searched for in the representative genes of the *P. aeruginosa* pangenome, with an e-value lower than 0.01 considered significant. We adopted a guilt-by-association approach to categorize the eukaryotic innate-like homologs into “near” and “remote” based on their distance to known phage defense systems. This classification was determined by their proximity within 100 kb of a known defense system. We established this threshold based on the bimodal distribution of distances between known defense systems in *P. aeruginosa* (Figure 1A). We then annotated the homologs found in *P. aeruginosa* using the Pfam-A HMM library and checked for enriched functional domains within the “near” defense island compared to “remote”. A subset of conserved gene clusters with these enriched functional domains were selected for further testing of antiviral activity. The

conservation of these gene clusters across species was further assessed using WebFlags v1.¹³⁹ In addition, the signal peptide and transmembrane regions were annotated with the use of SignalP v5.0¹³⁶ and Phobius v1.01.¹²⁹ All confirmed defense systems were checked for the presence of repeat regions using HHrepID.¹¹⁸ Regions of the proteins that remained uncharacterized were further analyzed using DALI⁴⁴ and Foldseek v6.⁸⁴ A confidence level higher than 90% and an e-value lower than 0.001 was considered significant.

Cloning of the putative eukaryotic-like defense systems

The putative eukaryotic-like defense systems were amplified from *P. aeruginosa* strains using primers from Table S6 with Q5 DNA Polymerase (New England Biolabs). PCR products were run on 1% agarose gels, and bands were excised and cleaned using the Zymoclean Gell DNA Recovery Kit (Zymo Research). Plasmid pUCP20 was digested with BamHI and EcoRI (NEB), treated with FastAP (Thermo Scientific), and cleaned with the Zymo DNA Clean & Concentrator Kit (Zymo Research). The defense systems were then cloned into the digested pUCP20 using the NEBuilder HiFi DNA Assembly Master Mix and transformed into chemically competent NEB® 5-alpha Competent *E. coli* following the manufacturer's instructions. Plasmids (Table S7) were extracted using the GeneJET Plasmid Miniprep kit and confirmed by sequencing (Macrogen). Confirmed plasmids were transformed into PAO1 by electroporation as previously described¹⁴³ and the cells were plated on LBA plates supplemented with 200 µg/ml of carbenicillin.

Selection for point mutations

A combination of strategies was employed to identify the amino acids to mutate in the defense system proteins. These included performing a literature search to identify known critical amino acids of the functional domains of the proteins, multiple protein alignments using PSI-BLAST¹³¹ and Clustal W v2.1¹¹² to identify conserved amino acids, and AlphaFold2^{104,105} 3D prediction to visually inspect active sites.

Cloning of knockout and point mutants of the defense systems

Gene knockouts and point mutations of the defense systems in pUCP20 were obtained by round-the-horn site-directed mutagenesis using phosphorylated primers (Table S6) and Q5 DNA Polymerase. PCR products were digested with DpnI (NEB), run on 1% agarose gels, and the bands were extracted and cleaned with the Zymo Gel DNA Recovery Kit. The amplified plasmids were ligated with T4 DNA ligase (NEB) at room temperature for 2 hours and transformed into chemically competent NEB 5-alpha Competent *E. coli* following the manufacturer's instructions. Plasmids were extracted using the GeneJET Plasmid Miniprep kit and confirmed by sequencing (Macrogen). Confirmed plasmids were transformed into PAO1 by electroporation as previously described.

Efficiency of plating

Phage stocks were 10-fold serially diluted in LB and the dilutions were spotted onto double layer agar plates of PAO1 with empty pUCP20 or pUCP20 with defense systems following the small plaque drop assay.¹⁴⁴ The anti-phage activity of the systems was calculated as the fold reduction of phage infectivity of the PAO1 strain that contains the pUCP20-encoded defense systems, compared to the infectivity of the PAO1 strain containing the empty plasmid.

Infection dynamics of phage-infected cultures

Bacterial cultures of PAO1 strains with empty pUCP20 or pUCP20 containing a defense system at an $OD_{600} \approx 0.1$ were infected with phage at an MOI < 1 and incubated at 37°C and 180 rpm. Samples were taken at 0h, 2h, 4h, and 6h, and centrifuged at $3,000 \times g$ for 5 min. The phage-containing supernatant was serially diluted and spotted onto DLA plates of PAO1 to estimate phage concentration.

Liquid culture collapse assays

Overnight bacterial cultures were diluted to an $OD_{600} \approx 0.1$ in LB and distributed into 96-well plates. Phages were added at MOIs of 0.01 and 10, and the plates were incubated at 37°C in an Epoch2 microplate spectrophotometer (Biotek) for OD_{600} measurements every 10 min for 24h, with double orbital shaking.

Screening for mutant phages that escape defense

Screening for mutant phages that evade defense was performed as previously described with minor adjustments.¹⁴⁵ Briefly, phages were 10-fold serially diluted and spotted onto DLA plates containing PAO1 strains expressing individual defense systems. After overnight incubation at 37°C, plates were examined for plaque formation. Single plaques were selected and transferred into LB, incubated for 1h at room temperature, and centrifuged at $8,000 \times g$ for 5 min to recover the phage-containing supernatant. The recovered phage suspensions were then serially diluted and spotted onto DLA plates containing PAO1 strains expressing either an empty pUCP20 vector or individual defense systems. Original phages were also diluted and spotted for comparison. Following overnight incubation at 37°C, the fold change in phage concentration between the negative control cells and those containing defense systems was determined.

LC-MS analysis

The LC-MS analyses were performed using an Agilent LC/MS system consisting of a high pressure liquid chromatography set-up coupled to a triple-quadrupole (QQQ) mass spectrometer (G6460C) equipped with a standard electrospray ionization (ESI) source.

Both systems were operated through MassHunter v10.1. The samples were randomized prior to their analysis. 3 μ l of each sample were injected into the column of the HPLC. Myo-inositol and inositol monophosphate were delivered to a CSH C₁₈ guard-column and a CSH C₁₈ column (Waters) (2.1 mm by 5 mm, 1.7- μ m pore size) at 30°C with a flow rate of 0.3 ml/min using the following binary gradient: 0% B (acetonitrile), ramp to 5% B in 5 min followed by a 6 min ramp to 75% B then a 1 min ramp back to 100% A (5 mM ammonium acetate) and 3 min re-equilibration (A, 20 mM ammonium formate). The metabolites eluting from the column were sprayed into the mass spectrometer operated in data-dependent mode, as in dynamic multiple reaction monitoring (dMRM) mode using transitions. The MRM transitions were generated by optimizing the fragmentor voltage and the collision energy. The dMRM was acquired in negative mode with a cycle time of 500 ms. Data processing was done using Skyline.¹³⁷ Peaks corresponding to myo-inositol and inositol monophosphate were integrated for quantification, and the area under the curves were exported for further analysis.

Phage adsorption kinetics in Hermes

Bacterial cultures of PAO1 strains containing pUCP20, pUCP20-Hermes, or pUCP20-Hermes D89A were grown until an OD₆₀₀ of 0.3, infected with phage ϕ Pa34 or ϕ Pa36 at an MOI of 0.1, and incubated at 37°C and 180 rpm. Samples were taken at 0, 10, 20, and 30 min post-infection and immediately centrifuged at 12,000 \times g for 1 min. The supernatant was serially diluted and spotted onto DLA plates of PAO1 to estimate the concentration of non-adsorbed phages.

Extraction and visualization of outer membrane protein

Outer membrane proteins were extracted from PAO1 strains containing pUCP20, pUCP20-Hermes, or pUCP20-Hermes D89A as previously described with slight modifications.¹⁴⁶ Overnight grown cultures were centrifuged at 10,000 \times g for 20 min, and the cell pellet re-suspended in 10 mM Tris-HCl pH 8.0. Cells were lysed using B-PER™ Bacterial Protein Extraction Reagent (Thermo Fisher Scientific) following manufacturer instructions. The supernatant was centrifuged at 21,000 \times g for 1 h at 15°C, and the cell pellet containing cytoplasmic and outer membranes was re-suspended in 10 mM Tris-HCl pH 8 containing 2% Sarkosyl. Samples were incubated in a rotary shaker at room temperature for 30 min and centrifuged at 21,000 \times g for 30 min at 15°C. The pellet was re-suspended in 10 mM Tris-HCl pH 8 containing 2% Sarkosyl and centrifuged again. The outer membrane pellet was then washed twice and re-suspended in 10 mM Tris-HCl pH 8. Protein concentration was determined using the Pierce BCA Protein Assay Kit (Thermo) according to manufacturer instructions and the samples run on a 4-12% SurePAGE, Bis-Tris gel (GenScript) at 200V in MOPS buffer (GenScript). The gel was stained with Bio-Safe Coomassie G-250 stain (Bio-Rad) and visualized on Bio-Rad Gel Doc XR+.

Extraction and visualization of lipopolysaccharides

LPS was extracted from *P. aeruginosa* PAO1 cells harboring pUCP20, pUCP20-Hermes, or pUCP20-Hermes D89A as previously described with minor modifications.¹⁴⁷ Briefly, overnight cell cultures were adjusted to an OD₆₀₀ of 0.5 in NaCl 0.9% (w/v). Cells were centrifuged at 10,600 \times g for 1 min and the pellet re-suspended in NaCl 0.9% and centrifuged again. The cell pellet was re-suspended in lysis buffer (1M Tris-HCl pH 6.8, 2% SDS, 4% 2-mercaptoethanol, 10% glycerol) and incubated at 95°C for 10 min. Proteinase K solution (25 μ g/ml proteinase K in lysis buffer) was added to cooled down samples and incubated at 56°C for 1 h with shaking. The solution was directly loaded onto a 4-12% SurePAGE, Bis-Tris gel and run at 20 mA in MOPS buffer. The gel was stained with the SilverQuest Silver Staining Kit (Thermo Scientific) following manufacturer instructions and imaged with Bio-Rad GelDoc XR+.

Extraction and visualization of capsule density

Bacteria were separated by capsule density using a discontinuous density gradient as previously described with minor adaptations.¹⁴⁸ Briefly, overnight cultures of *P. aeruginosa* PAO1 cells harboring pUCP20, pUCP20-Hermes, or pUCP20-Hermes D89A were centrifuged for 10 min at 3,200 \times g for 10 min, and the pellet re-suspended in 1X phosphate buffered saline (PBS). After centrifugation, the pellet was washed once more with 1X PBS, and re-suspended in 1 ml of 1X PBS. The cell suspension was added onto a discontinuous density gradient of 30%, 60%, 80% Percoll (w/v in 1XPBS, Sigma), and centrifuged for 30 min at 3,000 \times g for 30 min.

Phage adsorption to capsule and lipopolysaccharides

CPS and LPS were extracted from PAO1 strains containing pUCP20, pUCP20-Hermes, or pUCP20-Hermes D89A as previously described with slight modifications.¹⁴⁹ Briefly, overnight cell cultures were adjusted to an OD₆₀₀ of 0.65 and centrifuged at 12,000 \times g for 5 min. The cell pellet was re-suspended and vortexed in lysis buffer (60 mM Tris-HCl pH 8, 5 μ g/ml of CaCl₂, 2 mg/ml MgCl₂) containing 3 mg/ml lysozyme and incubated at 37°C for 1 h. Samples were then subjected to three cycles of freeze (-80°C) and thaw (37°C). DNase and RNase were added at 20 μ g/ml and incubated at 37°C for 30 min, followed by additional incubation with 0.1% SDS. Extractions were boiled at 100°C for 10 min, cooled down and mixed 2 mg/ml of proteinase K in lysis buffer. After incubation at 60°C for 1 h, extractions were centrifuged at 14,000 \times g for 2 min. The supernatant was recovered, mixed with cold 75% ethanol, and incubated at -20°C overnight. Extractions were centrifuged at 14,000 \times g for 30 min at 4°C and the CPS/LPS pellets resuspended in LB. The CPS/LPS pellets were 10-fold serially diluted and incubated with phage ϕ Pa34 at 10⁶ pfu/ml for 1 h at 37°C with shaking. The mixtures were 10-fold serially diluted and spotted onto DLA plates containing PAO1 to determine the amount of phage that did not adsorb to the CPS/LPS extracts.

Protein complex prediction

Predicted aligned error plots were generated with AlphaFold2 multimer^{104,105} for each hetero- and homomeric co-folded protein combination. Overlapping low predicted aligned error rates between proteins were seen as an indication for putative protein complex formation.

Phage R-loop prediction

QmRLFS-finder¹⁵⁰ was applied to predict the R-loop structures within the phage collection. Predicted R-loops were considered only if they were identified within a transcript and in the same transcriptional direction.

Comparison of IMPA, SuhB, and HrsA

We compared the structure of bacterial SuhB (*M. tuberculosis*, PDB: 2Q74) and eukaryotic Human IMPA (PDB: 1AWB) with the AlphaFold2 predicted structure of Hermes (WP_023087430.1) using DALI pairwise structure comparison. The alignments of these structures were further investigated using ChimeraX matchmaker.

RNA-seq experiments with Prometheus

Bacterial cultures of PAO1 strains containing pUCP20, Prometheus, and their mutants, were grown until an OD₆₀₀ of 0.3 and infected with phage at MOI of 1. Samples were taken pre-infection and at 20 min post infection and centrifuged at 5000 × *g* for 5 min at 4°C. RNA was extracted from the cell pellets using the RNeasy Mini kit and the RNase-free DNase set (Qiagen) following manufacturer's instructions. RNA concentration was determined using Qubit RNA High Sensitivity (HS) (Thermo), and the samples subjected to prokaryotic mRNA-seq (WOB) by Novogene (Cambridge, UK). Adapters (5' adapter: 5'-AGATCGGAAGAGCGTCGTGTAGGGAAAGAGTGTAGATCTCGGTGGTCGCCGTATCATT-3'; 3' adapter: 5'-GATCGGAAGAGCACACGTCTGAACTCCAGTCACGGATGACATATCTCGTATGCCGTCTTCTGCTTG-3') were removed from the reads and the reads filtered out if they contained an N content greater than 10%, or low-quality (Qscore ≤ 5) bases for more than 50% of the total bases. The remaining sequences were mapped on their corresponding reference genome using bwa v0.7.18.¹¹⁰ Subsequently, the number of reads per gene were determined using Samtools v1.20¹³⁴ in cohorts with bedtools intersect v2.31.1¹⁰⁸ and the NCBI genome annotation file (gff).^{115,116}

Sequencing during phage infection

Bacterial cultures of PAO1 strains containing pUCP20, Prometheus, and its mutants were grown until an OD₆₀₀ of 0.3 and infected with phage at MOI of 1. Samples were taken pre-infection and at 20 min post infection and centrifuged at 5000 × *g* for 5 min at 4°C. DNA was extracted from the cell pellets using the GeneJET Genomic DNA Purification Kit (Thermo Scientific) following manufacturer instructions. DNA was sequenced using Nanopore at Plasmidsaurus. Obtained reads were quality checked and the bottom 5% of reads with the lowest quality score reads removed via Filtlong v0.2.1 (default parameters). The filtered reads were mapped onto the corresponding reference genome of the phage and host using minimap2 v2.28¹²³ (map-ont parameter). The alignment statistics were obtained using Samtools v1.20 and visualized using Integrative Genomics Viewer (IGV).¹²⁰

NAD/NADH measurements

Bacterial cultures of PAO1 strains containing pUCP20, Thoeris III, and Thoeris III H49A SLOG were grown until an OD₆₀₀ of 0.3. Cultures were divided and one part infected with phage φPa34 at an MOI of 1 for 30 minutes. Uninfected and infected cultures were centrifuged at 5000 × *g* for 5 min at 4°C, and the pellet washed once with cold 1x PBS. The cell pellets were then used for NAD/NADH quantification using the NAD/NADH quantification kit (Sigma) following manufacturer instructions.

Building HMM models of the defense systems

HMM models for multi-gene defense systems were created using cblaster v1.3.18¹¹¹ to obtain all clusters within *P. aeruginosa* in which the defense genes were present and near each other (20% pident). Single-gene defense systems were searched for using PSI-BLAST¹³¹ search, and sequences with a pident lower than 20% and coverage lower than 70% were excluded. Muscle5¹²⁴ (-super5) was used to align the obtained protein sequences, and hmmbuild v3.3.2¹¹⁹ was used to build the HMM models. The HMM model scoring thresholds were set based on the 100% sensitivity-point with the help of an ROC curve analysis that scored the HMM sensitivity for the defense gene compared to all other genes within *P. aeruginosa*. The HMM bitscore obtained for each defense system gene is as follows: Prometheus *proA*, 3500; Hermes *hrsA*, 325; 6A-MBL *mbIB*, 130, and *cap2-3*, 230; Erebus *eruA*, 190; Hypnos *hypA*, 350; and Thoeris III *thcA*, 75, *thcB1*, 50, *thcB2*, 50, *thcB3*, 50, *thcB4*, 75, with the presence of *thcA* and *thcB4* genes being mandatory.

Search for novel defense systems in archaeal and bacterial genomes

To detect all prokaryotic homologs of the defense systems found in this study, we applied the HMM models on the proteins of all representative genomes, which were downloaded from RefSeq in February 2023. The taxonomy of each identified defense system is based on the annotation provided by RefSeq itself.

Phylogenetic tree and annotation of the defense system genes

Phylogenetic trees of ProA (Prometheus) and HrsA (Hermes) were made by obtaining all available Uniprot Release 2024_01¹⁵¹ protein sequences that contained DNA2 (n = 131,097) or IMPase (n = 56,571) functional domains, respectively. ATP-dependent DNA helicase

RecG protein (Genbank: NP_254032.1) and fructose-1,6-bisphosphatase class 1 (FBPase class 1; Genbank: CEI80039.1) were used to root the ProA and the HrsA phylogenetic trees, respectively. To generate the TIR and SLOG domain phylogenetic trees, all sequences of the corresponding protein clans, STIR (CL073, n = 108k) and SLOG (CL0349, n = 155k), were downloaded from the InterPro 98.0 database¹⁵² on February 6, 2024. Duplicate sequences were removed using Seqkit v2.7.0 (rmdup),¹³⁵ followed by a downsampling step (Seqkit sample). Representative sequences were obtained using mmseqs2 v15.6 (easy-cluster),¹²⁵ with the degree of downsampling based on the number of representatives obtained (between 1000 and 1500 sequences). The representative sequences were aligned using Muscle v5.3 (-super5)¹²⁴ and trimmed using trimAl v1.8 (-automated1).¹³⁸ The resulting trimmed alignment was used to build and bootstrap a phylogenetic tree using IQ-Tree2 v2.2.6¹²¹ (-B 1000, -alrt 1000, -m TEST). The phylogenetic tree of Hypnos and Erebus was built with the NACHT-containing NLR protein accessions and phylogenetic group information provided by Kibby et al.⁶⁷ (n = 3247). These sequences were aligned using Muscle v5.3 (-super5), trimmed using trimAl v1.8¹³⁸ (-automated1), and a phylogenetic tree was built using FastTree v2.1.11¹¹⁷ with default settings. All phylogenetic trees were visualized using iTOL v1.0.¹⁵³

Phylogeny tree of *Pseudomonas aeruginosa*

A phylogenetic tree was constructed using Parsnp v1.7.4¹²⁸ on all complete *P. aeruginosa* assemblies from the Refseq database on June 16, 2022 (n = 541) and visualized using iTOL.¹²²

QUANTIFICATION AND STATISTICAL ANALYSIS

Unless stated otherwise, data are presented as the mean of biological triplicates \pm standard deviation. A Bonferroni-adjusted p-value of less than 0.05 was considered significant.